

Quaternary slip-rates of the Kazerun and the Main Recent Faults: active strike-slip partitioning in the Zagros fold-and-thrust belt

Christine Authemayou, Olivier Bellier, Dominique Chardon, Lucilla Benedetti, Zaman Malekzade, Christelle Claude, B Angeletti, Esmaeil Shabanian

▶ **To cite this version:**

Christine Authemayou, Olivier Bellier, Dominique Chardon, Lucilla Benedetti, Zaman Malekzade, et al.. Quaternary slip-rates of the Kazerun and the Main Recent Faults: active strike-slip partitioning in the Zagros fold-and-thrust belt. Geophysical Journal International, 2009, 178 (1), pp.524-540. 10.1111/j.1365-246X.2009.04191.x . insu-00418700

HAL Id: insu-00418700
https://insu.hal.science/insu-00418700

Submitted on 12 Mar 2021

HAL is a multi-disciplinary open access archive for the deposit and dissemination of scientific research documents, whether they are published or not. The documents may come from teaching and research institutions in France or abroad, or from public or private research centers.

L'archive ouverte pluridisciplinaire **HAL**, est destinée au dépôt et à la diffusion de documents scientifiques de niveau recherche, publiés ou non, émanant des établissements d'enseignement et de recherche français ou étrangers, des laboratoires publics ou privés.

Geophys. J. Int. (2009) **178,** 524–540 doi: 10.1111/j.1365-246X.2009.04191.x

Quaternary slip-rates of the Kazerun and the Main Recent Faults: active strike-slip partitioning in the Zagros fold-and-thrust belt

Christine Authemayou,[1,*] Olivier Bellier,[1] Dominique Chardon,[1,†] Lucilla Benedetti,[1] Zaman Malekzade,[2] Christelle Claude,[1] Bernard Angeletti,[1] Esmaeil Shabanian[1,2] and Mohammad Reza Abbassi[2]

[1]*Centre Européen de Recherche et d'Enseignement de Géosciences de l'Environnement (CEREGE, UMR CNRS – Aix-Marseille Université, IRD et collège de France), Université Paul Cézanne,* BP 80, 13545 *Aix-en-Provence Cedex* 4*, France. E-mail: christine.authemayou@univ-breat.fr*
[2]*International Institute of Earthquake Engineering and Seismology, Sholeh str.,* 8th *Kohestan, Pasdaran, Tehran, I.R., Iran*

Accepted 2009 March 19. Received 2009 March 16; in original form 2008 August 21

SUMMARY

The aim of this work is to constrain the Late Quaternary activity of two major dextral strike-slip faults of the Zagros fold-and-thrust belt of Southern Iran, within the framework of right-oblique convergence between Arabia and Eurasia. The NW-trending Main Recent fault marks the rear of the belt along two thirds of its length. Its southeastern tip connects to the northern termination of the N-trending Kazerun Fault, which affects the entire width of the belt. Horizontal slip rates have been estimated on these two faults over the last 140 ka from lateral offsets of streams and fans and *in situ* cosmogenic ^{36}Cl exposure dating of cobbles sampled on the surface of these geomorphic features. Compared to GPS data, the obtained minimum slip rate of 3.5–12.5 mm yr^{-1} on the Main Recent Fault implies strike-slip partitioning of the convergence along this fault. Minimum slip rate of the Kazerun Fault is 2.5–4 mm yr^{-1} for its northern strand, 1.5–3.5 mm yr^{-1} for its central segment and is negligible for its southern segment. These results are consistent with southward distribution of the slip from along the Main Recent Fault to the longitudinal thrusts and folds of the fold-and-thrust belt through the Kazerun Fault, with a decrease of slip from the southeastern tip of the Main Recent Fault towards the southern termination of the Kazerun Fault. The Kazerun and associated faults form the horsetail termination of the Main Recent fault and may be seen as the propagating southeastern front of the fault system that accommodates indentation of Eurasia by Arabia.

Key words: Seismicity and tectonics; Continental neotectonics; Continental tectonics: strike-slip and transform; Tectonics and landscape evolution.

GJI Tectonics and geodynamics

Downloaded from https://academic.oup.com/gji/article/178/1/524/2069791 by guest on 12 March 2021

1 INTRODUCTION

The Zagros fold-and-thrust belt results from the collision between Arabia and Eurasia (Fig. 1a). The plate convergence vector has a N- to NNE-trending direction, approximately 45° oblique to the general trend of the western and central Zagros and normal to the trend of the eastern Zagros (e.g. Vernant *et al*. 2004a; Fig. 1b). The accommodation mode of convergence therefore varies longitudinally due to the along-strike variation of the convergence obliquity (Talebian & Jackson 2004). The transition from oblique (western Zagros) to pure shortening (eastern Zagros) occurs in the vicinity of the junction between two major right-lateral strike-slip faults of the Middle-East collision belt. These are the NW-trending Main Recent Fault (MRF), forming the northeastern boundary of the western Zagros, and the N-trending Kazerun Fault (KF) that cuts across the entire width of the belt (Fig. 1b; Authemayou *et al.* 2005).

Geodetically and long-term, geologically derived slip rates on the MRF range from 1.2 to 17 mm yr^{-1} (Talebian & Jackson 2002; Bachmanov *et al*. 2004; Vernant & Chéry 2006; Walpersdorf *et al.* 2006). Besides the fact that instantaneous and long term slip rates are integrated over different time windows, this wide range of values might be due (1) to the poorly constrained age of slip initiation on the fault and (2) to the degree of strike-slip partitioning ascribed to the fault in accommodating geodetically measured across-strike shortening rates of the fold-and-thrust belt (Vernant & Chéry 2006). Geologically derived slip rate on the KF has not yet been rigorously determined. The aim of the present paper is to determine the slip rates on the southeastern strands of the MRF (between 50°E and 52°E) and along the KF over an intermediate time scale (i.e. the Late Quaternary). Slip rates were determined by combining measurements of fault offsets of geomorphic features such as stream

*Now at: Université Européenne de Bretagne, France; Université de Brest, CNRS, Laboratoire "Domaines océaniques", UMR 6538-IUEM, Place Copernic, Plouzané, France.
†Now at: Université de Toulouse, UPS (OMP), LMTG, 14 avenue Edouard Belin, 31400 Toulouse, France.

© 2009 The Authors
Journal compilation © 2009 RAS

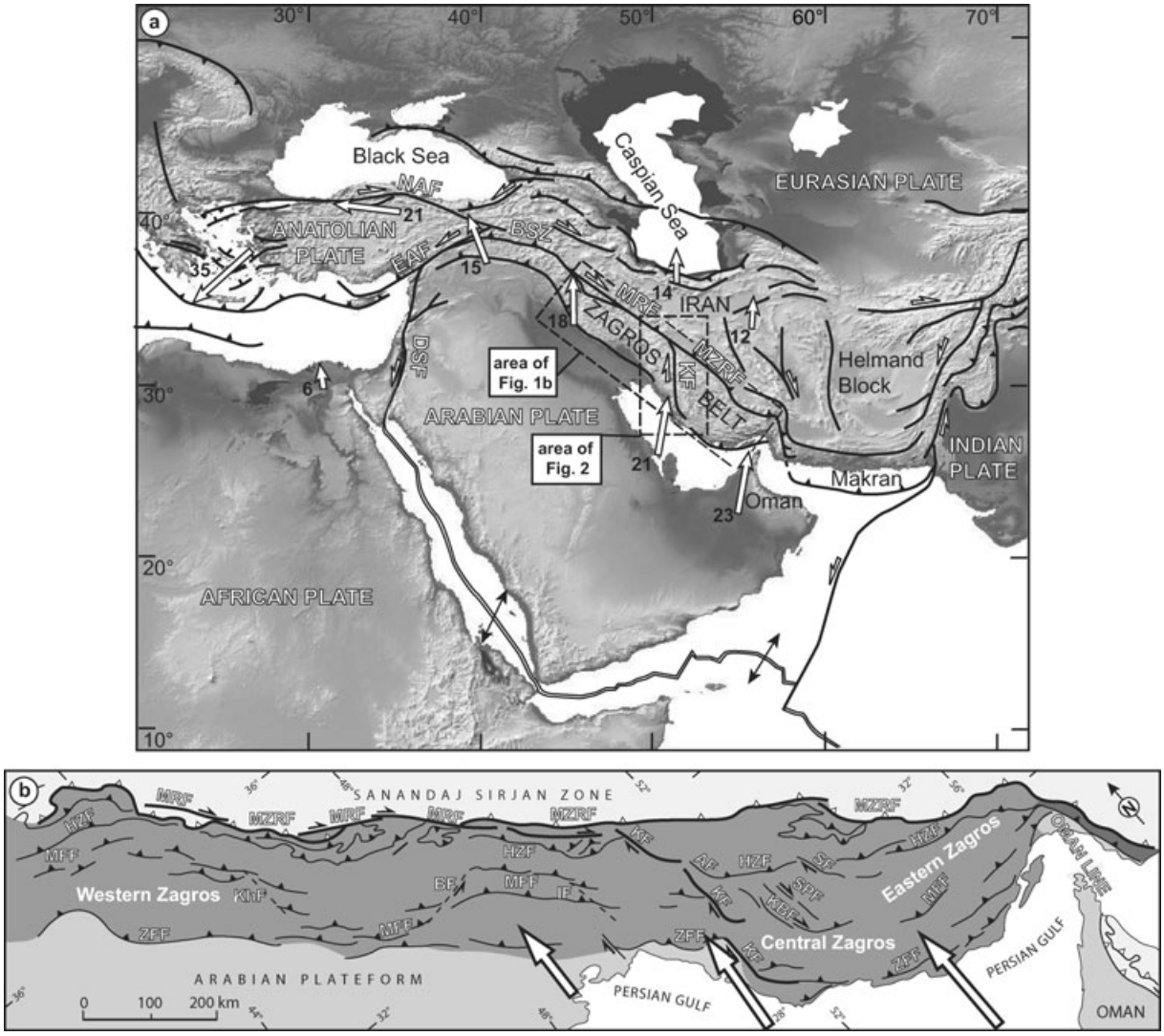


Figure 1. (a) Structural frame of the Middle East Alpine collision belt. White arrows indicate velocity vectors with respect to stable Eurasia (Reilinger *et al.* 1997; Vernant *et al.* 2004a). Velocities are given in mm yr^{-1}. BSZ, Bitlis Suture Zone; DSF, Dead Sea fault; EAF, East Anatolian fault; KF, Kazerun fault; MRF, Main Recent fault; MZRF, Main Zagros reverse fault; NAF, North Anatolian fault. (b) Structural map of the Zagros fold-and-thrust belt (after Berberian 1995). Computed shortening rates across the belt (Vernant *et al.* 2004a) are shown. AF, Ardakan fault; BF, Balarud fault; HZF, High Zagros fault, IF, Izeh fault; KhF, Khanaqin fault; KBF, Kareh Bas fault; MFF, Main Frontal fault; SF, Sarvestan fault; SPF, Sabz Pushan fault; ZFF, Zagros Frontal fault (Stöcklin 1968; Falcon 1974).

channels and alluvial fans with their abandonment ages, which were estimated using cosmogenic ^{36}Cl surface exposure dating. The results allow constraining slip rates integrated over the past 140 ka. Slip rates are of 3.5–12.5 mm yr^{-1} on the MRF and decrease on the KF from 2.5–4 mm yr^{-1} on its northern segment to 1.5–3.5 mm yr^{-1} on its central segment to become negligible on its southern segment. Compared to GPS data, these results require a large degree of partitioning of oblique plate convergence across the Western Zagros along the MRF. The southward decrease in the slip rate on the KF is also consistent with slip from along the MRF being transmitted to the KF and subsequently to the thrust ramps and folds of the belt through the thrust terminations of the various strands of that fault.

2 SEISMOTECTONIC SETTING AND PREVIOUS WORKS

The NW-trending Zagros fold-and-thrust belt results from the collision between the Arabian plate and the Central Iran micro continents accreted onto the Eurasian plate during the Meso-Cenozoic (Falcon 1969, 1974; Haynes & McQuillian 1974; Stöcklin 1974; Berberian & King 1981). The northeastern backstop of the belt is marked by the suture zone that coincides with a major thrust, the Main Zagros Reverse Fault (MZRF), which is presently inactive (Fig. 1b; Berberian & King 1981; Jackson & Mc Kenzie 1984; Tatar *et al*. 2002; Yamini-fard *et al.* 2006). GPS measurements indicate that the Arabian and Eurasian plates converge with an N- to NNE-trending direction (e.g. Vernant *et al.* 2004a; Hessami *et al*. 2006). The geodetically determined shortening rate across the Zagros varies from 4.5 $\pm$ 2 mm yr^{-1} in the northwest to 9 $\pm$ 2 mm yr^{-1} in the southeast. This variation results from the anticlockwise rotation of the Arabian plate (Jackson & McKenzie 1988; Vernant *et al*. 2004a).

The MRF is one of the major right-lateral faults of the Middle-East collision belt, which stretches from easternmost Anatolia to *ca*. 51°E, parallel to the Zagros suture zone (Fig. 1b; Talebian & Jackson 2002). The fault may be seen as a southeastern extension of the North Anatolian Fault (Ricou *et al.* 1977; Jackson & McKenzie

© 2009 The Authors, *GJI*, **178,** 524–540
Journal compilation © 2009 RAS

Downloaded from https://academic.oup.com/gji/article/178/1/524/2069791 by guest on 12 March 2021

1984) although the MRF and the North Anatolian Fault are separated by major discontinuities south of the Caucasus (Talebian & Jackson 2002; Fig. 1a). At its southeastern termination, the MRF branches on to the KF, which stretches from the southeastern tip of the MRF to the Persian Gulf (Authemayou *et al*. 2005). Fault-slip data analysis, tectonic geomorphology and earthquake focal mechanisms attest to a long-term to active dextral strike-slip regime along the MRF (Tchalenko & Braud 1974; Berberian 1995; Berberian & Yeats 2001; Talebian & Jackson 2002; Bachmanov *et al*. 2004; Yamini-Fard *et al*. 2006; Peyret *et al*. 2008). Southwest of the MRF, thrust faults have coseismic slip vectors striking normal to the structural trend of the belt (Talebian & Jackson 2004). This, together with the fact that the focal mechanisms along the MRF show pure strike-slip movements, suggests that oblique convergence is completely partitioned along this part of the MRF (Talebian & Jackson 2004). Complete partitioning of the oblique convergence over the long-term is yet to be confirmed.

Talebian & Jackson (2002) have documented a 50-km-long cumulated horizontal offset along the MRF. Assuming that the MRF formed 3–5 Myr ago, the authors calculated a slip rate of 10–17 mm yr^{-1} on the fault. They correlate the formation of the MRF with the onset of the major shortening phase documented in the Zagros (Stöcklin 1968; Falcon 1974; Stoneley 1981) as well as with a regional re-organisation of the Middle-East collision zone (e.g. Allen *et al*. 2004). Moreover, Authemayou *et al.* (2006) provided geological evidence that the fault cuts across faults and folds that were active during sedimentation of the Lower Baktiary Formation, this formation being considered as Lower Pliocene in age (James & Wynd 1965). This would therefore imply an early Pliocene age for the onset of the right-lateral slip along the MRF, in agreement with Talebian & Jackson (2002) interpretation. By assuming 10–15-km of right-lateral displacement of early Pliocene pull-apart basins, Copley & Jackson (2006) derive a slip rate of 2–5 mm yr^{-1} along the MRF close to its northwestern termination. Considering the offset of river valleys incised into a planation surface of supposedly postglacial age, Bachmanov *et al*. (2004) have derived a 10 mm yr^{-1} slip rate for the MRF around 49°E (Fig. 2).

Instantaneous slip rate along the MRF deduced from GPS measurements (Vernant *et al*. 2004a) would be of 5 ± 1.5 mm yr^{-1} if the fault is considered to achieve total partitioning of the 7 ± 2 mm yr^{-1} of N–S shortening measured around 50°E. Based on local GPS network surveys, Walpersdorf *et al.* (2006) suggest 4–6 mm yr^{-1} of cumulated right-lateral strike-slip across the whole eastern Zagros. The range of published estimates for the slip rate along the MRF therefore varies from 1.2 to 17 mm yr^{-1}, calling for refinement based on Quaternary, precisely dated offset along the MRF (Talebian & Jackson 2002; Vernant & Chéry 2006).

The KF is a N-trending right-lateral fault that separates the Central and eastern Zagros in the vicinity of 51°E. The fault bounds to the west a set of transverse-oblique right-lateral strike-slip faults that are arranged into a fan-shaped fault pattern (Authemayou *et al*. 2005; Fig. 1b). The KF is made of three N-trending segments that branch southward on the NW-trending thrusts and ramp anticlines of the eastern Zagros (Fig. 2).

The historical and instrumental seismicity of the KF concentrates along its central segment (Baker *et al*. 1993; Berberian 1995; Talebian & Jackson 2004), where several historical events of intensity greater than 8 have been reported (Berberian & Tchalenko 1976). Cumulated offsets and derived slip rates along the KF are poorly constrained due to the lack of piercing points. The 140 km of apparent offset of a major reverse fault across the KF was used by Berberian (1995) to compute a slip rate of 14.5 mm yr^{-1} since the Late Miocene. However, this thrust is not necessarily the same synchronous structure on either side of the KF or may even be an originally bent structure. Based on local GPS network data, Walpersdorf *et al*. (2006) determined a slip rate of 6 ± 2 mm yr^{-1} across the whole fan-shaped right-lateral strike-slip fault system of the central Zagros with 2 mm yr^{-1} restricted to the KF. A more recent geodetic survey of the KF provides a dextral strike-slip motion of 3.7 ± 0.8 mm yr^{-1} along the northern segment, 3.6 ± 0.6 mm yr^{-1} along the central segment and negligible displacement along the southern segment (Fig. 2; Tavakoli *et al*. 2008).

Fault Kinematics analyses, seismicity and morphotectonic observations indicate that the KF and associated faults of the fan shaped pattern are active right-lateral strike-slip structures (Fig. 2). Authemayou *et al*. (2006) propose that they distribute slip from along the MRF towards the interior of the Zagros fold-and-thrust belt. This would be achieved through the connection between the MRF and the KF and the bent thrust terminations of each segment of the KF and associated faults. Such a kinematic model requires that the KF horizontal slip rate decreases southward because of the transfer of strike-slip to the thrust ramps of the belt.

3 MATERIALS AND METHODS

3.1 Tectonic geomorphology

Active fault traces of the MRF and KF were investigated by field mapping as well as from 1:50 000 scale, 20 m contour intervals topographic maps and geological maps analyses, which complemented the interpretation and analysis of orthorectified, 10 and 5 m resolution panchromatic SPOT images, 15 m resolution Visible Near Infrared ASTER images, and the SRTM-90 digital elevation model. These georeferenced data were compiled in Arcgis 9.2 Geographical Information System software. In the following, we used the term segment instead of that of fault zone, as suggested in the fault segmentation nomenclature (Schwartz & Sibson 1989), in order to be in agreement with the Iranian geology terminology (e.g. Berberian 1995). Typical tectonic landforms associated with active strike-slip faulting, such as deflected or offset stream channels, offset ridges, offset alluvial fan and fault scarps, are recognized along the MRF and the KF. These features were plotted in ARCGIS software from topographic maps and satellite images. When the numerical database was insufficiently precise to digitize the features, we used differential GPS field surveys to map them precisely. Displaced alluvial fans or distorted/offset drainage incised into the fans have been used to evaluate horizontal offsets of the two faults at several favourable sites (Fig. 2).

3.2 ^{36}Cl exposure dating

To derive a lateral slip rate on the MRF and the KF, we have determined *in situ*-produced ^{36}Cl exposure age of carbonate boulders sampled on the surfaces of faulted fans or terraces (Fig. 3). In carbonate rocks, *in situ* ^{36}Cl is produced primarily by interaction of cosmic rays neutrons and muons with Ca and Cl. Although production by thermal and epithermal neutrons from Cl is maximum at 20–50 cm depth, the total production rate can be described as an exponential decrease with depth with *in situ* ^{36}Cl that mostly accumulated at the surface (Gosse & Phillips 2001). The accumulation of a cosmogenic nuclide in a rock at the surface with time follow

Downloaded from https://academic.oup.com/gji/article/178/1/524/2069791 by guest on 12 March 2021

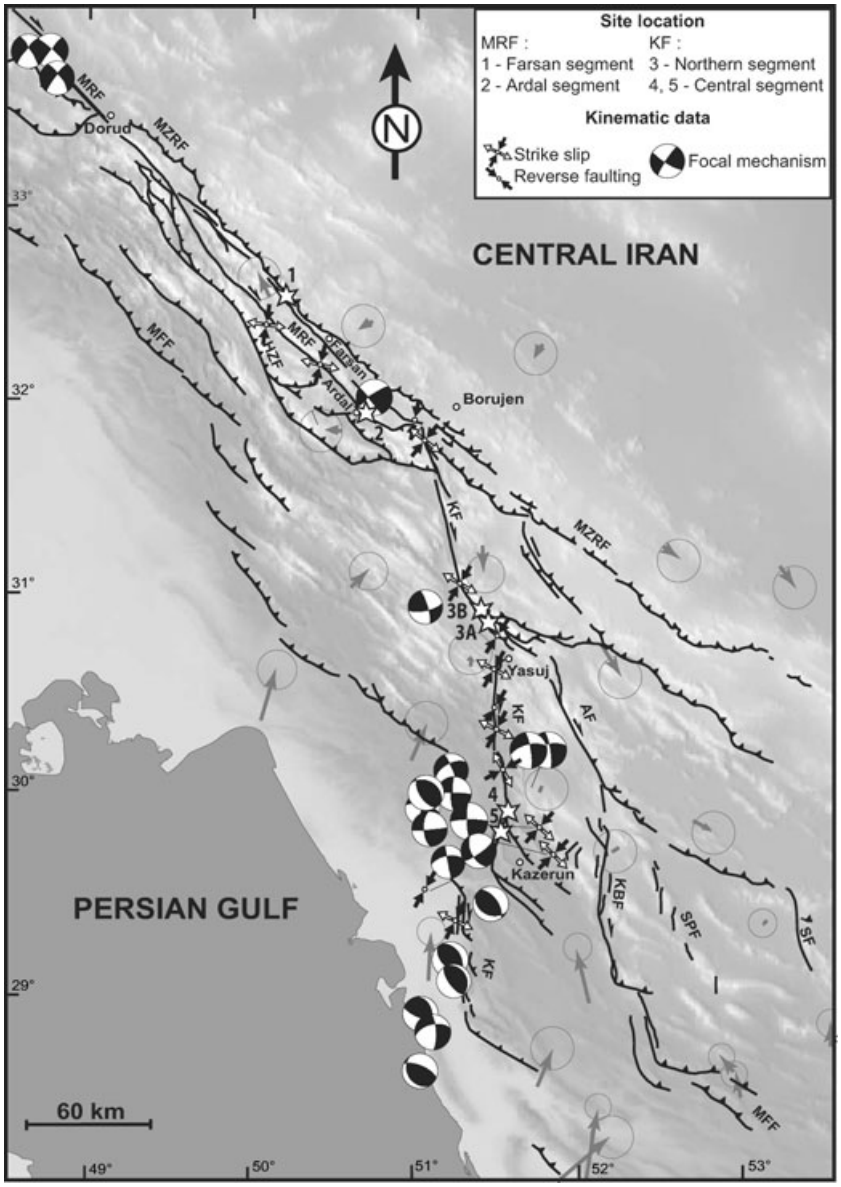


Figure 2. Traces of major active faults in the Central Zagros superimposed on the GTOPO 30 digital elevation model. Stars designate study sites. See Fig. 1 for fault nomenclature. Grey arrows indicate the GPS velocities with respect to Central Iran with their confidence ellipses (Tavakoli *et al.* 2008). Focal mechanisms are from the Havard catalogue (http://www.globalcmt.org/CMTsearch.html) and fault slip data inversion results from Authemayou *et al.* (2006).

this equation:

$$N(t) = N(0)\mathrm{e}^{-\lambda t} + \frac{P}{\lambda + \varepsilon\mu}[1 - \mathrm{e}^{-(\lambda+\varepsilon\mu)t,}]$$

where $N(t)$ is the concentration at time t (yr), P is the surface production rate (atom per g yr^{-1}), λ is the decay constant of the radioactive nuclide (2.303 10^{-6} yr^{-1}), ε is the erosion rate (cm yr^{-1}), μ is the absorption coefficient (cm^{-1}), equal to ρ/L, where ρ is the density of the sampled rock (2.7 g cm^{-3} for carbonate rocks) and L is the absorption mean free path for interacting cosmic secondary particles in the rock (160 g cm^{-2}). $N(0)$ is the inheritance component.

After separation of the cobbles from the surrounding calcrete (Fig. 3), the samples were grinded, leached and chlorine was chemically extracted by precipitation of silver chloride. The chemistry was done in CEREGE (CNRS, Aix-en-Provence). ^{36}Cl and chloride concentration in the carbonate was determined for all samples by isotope dilution accelerator mass spectrometry at the Lawrence Livermore National Laboratory CAMS facility. Blanks were two orders of magnitude lower than the samples and replicates were within less than 5 per cent similar. Surface exposure ages were calculated using ^{36}Cl production rates from calcium and chlorine of Stone *et al.* (1998) for all relevant pathways. Other published production rates (Swanson & Caffee 2001, and references therein) are higher than the Stone *et al*. (1998) value and would lead to younger ages (by about 20 per cent). Those production rates were calculated at our site latitude and altitude using Stone (2000) coefficients. The exposure ages presented in Table 1 include analysis and processing errors, as well as error on Stone *et al.* (1998) production rate. We have sampled on the zones least incised by streams and far enough from the fan apex to avoid younger overlying deposits. If we assume no inheritance and no erosion, ^{36}Cl cosmogenic concentration is interpreted to give a minimum surface exposure age (Cerling & Craig 1994). The common presence of calcrete cementing the surface of

© 2009 The Authors, *GJI*, **178,** 524–540
Journal compilation © 2009 RAS

Downloaded from https://academic.oup.com/gji/article/178/1/524/2069791 by guest on 12 March 2021

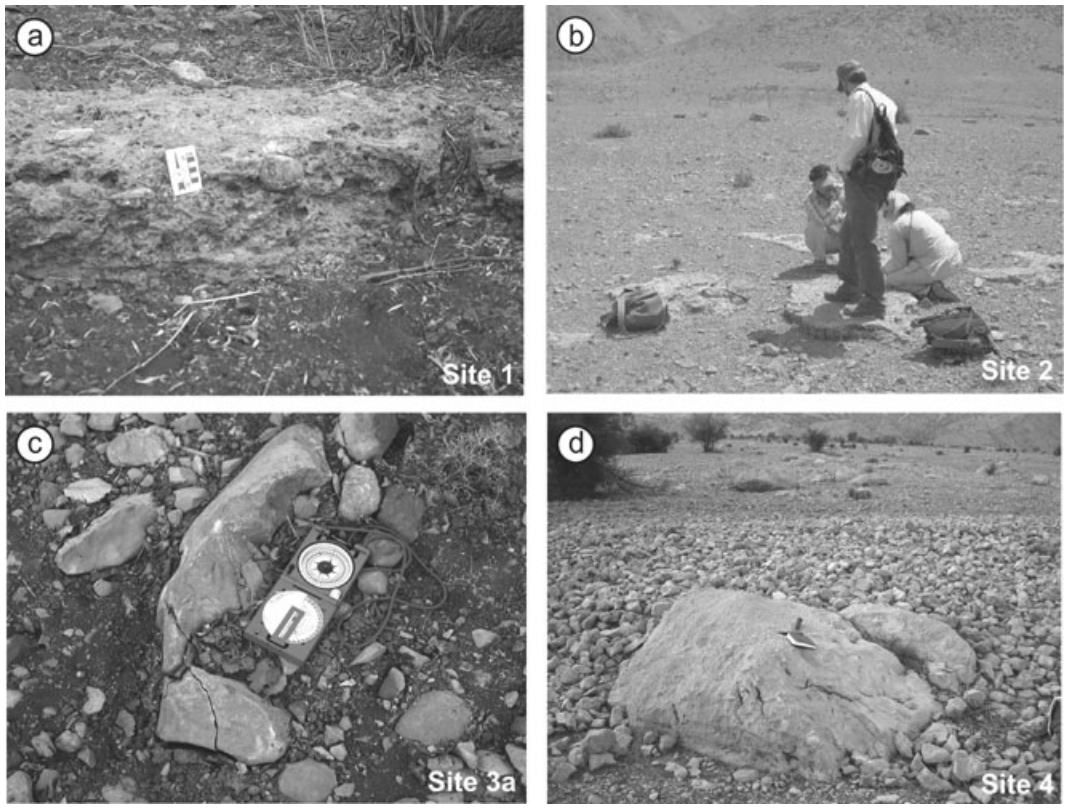


Figure 3. Views of the geomorphic surfaces sampled for ^{36}Cl dating. (a) Pebbles cemented by the calcrete topping the fan deposits at site 1 (g on Fig. 4b). (b) View of sampled indurated surface of the eastern fan at site 2 (h on Fig. 6a). (c) View of a pebble sampled on the fan-terrace surface at site 3a (q on Fig. 7a). (d) View of a boulder sampled on the fan surface at site 4 (× on Fig. 11a).

several of the fans (sites 1, 2 and 3a), together with the well preserved shape of the envelop of the fans further argues for a limited to negligible erosion of their abandonment surfaces.

4 SLIP RATES ON THE MAIN RECENT FAULT

We have investigated the two main strands of the southeastern part of the MRF between 50 and 52°E. Southeast of Dorud, the fault cuts through the mountain range and splits around 49°30′E into two strands, referred to as the Farsan and Ardal segments (Fig. 2). The segments are parallel and 10–15 km apart. They merge again around 51°E near Borujen, in the vicinity of the junction between the MRF and the KF.

4.1 Farsan segment (site 1, 32°33′29 N, 50°13′38 E)

Site 1 is located in the central part of the Farsan segment. The fault induced hectometric offsets of alluvial fans and the distortion of a channel network incising their surface (Fig. 4). In order to determine the tectonic offset of these features, a geomorphologic interpretation of 10 m-resolution orthorectified SPOT images and 1/50,000-scale topographic map was coupled with detailed field geological and morphometric analyses. The 20-m contour intervals of the topographic map combined with a histogram treatment by standard deviation of the satellite image enabled to individualize two alluvial fans (Fig. 4b). These fans are incised by a channel network 10–25 m deep. The channels are laterally distorted/offset by the fault (Fig. 4b). A consistent offset of *ca.* 160 m is measured on the SPOT image for six channels (Fig. 4b), suggesting that these streams have been deflected by the fault over the same period. As the lateral offsets of the fans' map boundaries have been smoothed out by erosion and are not clear-cut anymore (e.g. northern boundary of the southern fan), offsets of the channel network were used to evaluate minimum post-fans lateral slip on the fault (Fig. 4b). For improving the accuracy in the offset value determination, we have undertaken differential GPS surveys to map precisely with decimetric precision the trace of one of the distorted channel beds (Fig. 4c). The error in the offset measurement is considered as the uncertainty in the projection of the non-rectilinear streams to fault trace (Fig. 4c; Tibaldi & Leon 2000). A horizontal stream offset of 180 ± 33 m is deduced from the differential GPS data (Fig. 4c).

We collected seven pebbles taken into in the capping calcrete of the fan for ^{36}Cl exposure dating (Figs 3a and 4b). Shielding by the surrounding topography was measured in the field and found to be negligible. Assuming no erosion or inheritance, exposure ages range between 41 ± 5 and 143 ± 16 ka (Fig. 5, Table 1); five samples yield exposure ages between 41 ± 5 and 62 ± 7 ka whilst two samples give older ages (Fig. 5a). These two latter samples (number a and b) have anomalously high ^{36}Cl concentrations, suggesting that a portion of the measured concentration contains inherited ^{36}Cl produced by cosmic ray exposure before deposition, during or before alluvial transport (e.g. Daeron *et al*. 2004). Furthermore, as our aim is to date the abandonment of the fan surface, the group of age the most representative of the samples favours a fan exposure age between 36 and 69 ka (Fig. 5). This exposure age range combined with the measured channel offset of 180 ± 33 m leads to a slip rate of 2.1–5.9 mm yr^{-1}. This is a minimum slip rate since the tectonic offsets post-date the fan abandonment.

Downloaded from https://academic.oup.com/gji/article/178/1/524/2069791 by guest on 12 March 2021

Table 1. Sample characteristics and exposure ages.

Site Site	Altitude (m)	Latitude (°N)	Sample	Ca dissolved (g)	Cl (ppm)	^{36}Cl [10^5 atoms (g rock)$^{-1}$]	Production [atoms (g rock)$^{-1}$ yr^{-1}]	Age (10^3 yr)
Site 1	2390	32.56	a	9.79	32	74.28 ± 0.85	60.79 ± 6.08	143 ± 16
Site 1	2389	32.56	b	12.04	26	74.86 ± 0.85	87.19 ± 8.72	96 ± 11
Site 1	2380	32.56	c	12.61	24	50.58 ± 0.63	100.28 ± 10.03	54 ± 6
Site 1	2370	32.56	d	12.82	48	51.91 ± 0.59	97.79 ± 9.78	57 ± 6
Site 1	2385	32.56	e	11.41	23	52.26 ± 0.67	90.55 ± 9.05	62 ± 7
Site 1	2383	32.56	f	11.13	28	34.55 ± 0.50	88.03 ± 8.80	41 ± 5
Site 1	2370	32.56	g	10.69	27	41.33 ± 0.61	75.02 ± 7.50	59 ± 7
Site 2	2063	31.92	h	11.13	53	81.26 ± 0.97	67.04 ± 6.70	142 ± 16
Site 2	2080	31.92	i	7.56	265	151.24 ± 1.83	62.39 ± 6.24	355 ± 40
Site 2	2078	31.92	j	12.13	51	83.12 ± 0.90	71.29 ± 7.13	136 ±15
Site 2	2090	31.92	k	7.21	296	153.55 ± 1.96	71.66 ± 7.17	295 ± 33
Site 2	2078	31.92	l	13.56	67	102.44 ± 1.17	86.75 ± 8.68	138 ± 15
Site 2	2080	31.92	m	6.70	213	107.87 ± 1.33	57.35 ± 5.73	247 ± 28
Site 2	2078	31.92	n	5.93	64	99.80 ± 0.20	78.26 ± 7.83	151 ± 18
Site 3a	2110	30.84	o	12.17	36	66.63 ± 0.72	70.91 ± 7.09	106 ± 12
Site 3a	2105	30.84	p	12.71	23	69.16 ± 0.17	68.25 ± 6.83	115 ± 14
Site 3a	2100	30.84	q	12.23	51	74.16 ± 0.58	77.27 ± 7.73	108 ± 12
Site 4	993	29.88	r	13.01	101	12.30 ± 0.32	39.78 ± 3.98	32 ± 4
Site 4	993	29.88	s	13.31	88	16.50 ± 0.41	39.38 ± 3.94	44 ± 6
Site 4	978	29.88	t	9.61	321	13.51 ± 0.33	42.02 ± 4.20	33 ± 4
Site 4	964	29.88	u	11.86	83	9.01 ± 0.21	37.19 ± 3.72	25 ± 3
Site 4	966	29.88	v	12.14	172	18.73± 0.37	43.36 ± 4.34	45 ± 5
Site 4	968	29.88	w	11.85	213	24.61± 4.33	48.72 ± 4.87	54 ± 6
Site 4	973	29.88	x	12.81	54	9.90± 0.21	37.64 ± 3.76	27 ± 3

Site	Altitude (m)	Latitude (°N)	Depth (cm)	Ca dissolved (g)	Cl (ppm)	^{36}Cl [10^5 atoms (g rock)$^{-1}$]
Site 2 profil	2 090	31.92	0	7.11	139.99	32.51 ± 0.50
Site 2 profil	2 090	31.92	50	8.51	282.83	52.01 ± 1.01
Site 2 profil	2 090	31.92	100	8.37	390.05	40.12 ± 0.79
Site 2 profil	2 090	31.92	150	8.50	281.25	21.26 ± 0.53
Site 2 profil	2 090	31.92	200	8.22	296.57	13.96 ± 0.40
Site 2 profil	2 090	31.92	240	15.49	202.85	8.57 ± 0.29
Site 2 profil	2 090	31.92	300	7.78	260.15	5.52 ± 0.15
Site 3a profil	2 100	30.84	0	15.90	79.25	42.49 ± 0.67
Site 3a profil	2 100	30.84	50	16.08	38.45	18.14 ± 0.47
Site 3a profil	2 100	30.84	100	13.96	49.72	13.52 ± 0.30
Site 3a profil	2 100	30.84	150	15.95	91.91	10.60 ± 0.25
Site 3a profil	2 100	30.84	200	14.69	53.40	5.53 ± 0.13
Site 3a profil	2 100	30.84	250	15.26	46.54	3.77 ± 0.09
Site 3a profil	2 100	30.84	300	15.55	49.30	3.07 ± 0.08

Notes: ^{36}Cl and Cl concentrations from isotope dilution accelerator mass spectrometry for each surface samples and for the depth profiles samples with site characteristics. Exposure ages were calculated including all sources of production and assuming no erosion and no inheritance (Stone *et al.* 1998). The minimum exposure ages have been calculated using ^{36}Cl production rates from calcium of Stone *et al*. (1998) with altitude- and latitude scaling factors for neutrons and muons from Stone (2000). Calcium content in each sample was measured by ICP at CEREGE. ^{36}Cl measurements were standardized relative to NIST ^{36}Cl standard.

4.2 Ardal segment (site 2, 31°55′00 N, 50°44′78 E)

4.2.1 Offsets

At site 2, the Ardal segment cuts across upstream watershed basins of two large alluvial fans (Figs 2 and 6). The fault affects the source stream channel of the eastern fan whereas it displaces the apex of the western fan from its source valley (Fig. 6). This observation suggests that the offset postdates fan emplacement. We have analysed these two fans using field data and 5 m resolution SPOT image (Fig. 6a). The surface of the fans is capped by an at least 50-cm-thick calcrete that allowed good preservation of the original surface shape despite their dissection (e.g. the 80-m-deep canyon across the eastern fan; Fig. 3b). The two fans are considered as contemporaneous on the basis of their size, topography, dissection pattern, and the material they contain. Furthermore, the two fans do not show evidence for diachronous emplacement such as cut-and-fill structures.

In order to measure the cumulative offset of the western fan with respect to its feeder valley, the location of the fan's apex must be determined. Based on the assumption that the fan's contours are circular arcs having their curvature centres coinciding with the apex of the fan (e.g. Keller *et al.* 2000 and references therein), one obtains four apex locations from four 20 m contours, with a dispersion of 150 m (Fig. 6b). The location of the fan's feeder valley against the fault trace is deduced from mapping the valley using 5 m resolution SPOT images (Fig. 6b). In fact, this point must be located between

© 2009 The Authors, *GJI*, **178,** 524–540
Journal compilation © 2009 RAS

Downloaded from https://academic.oup.com/gji/article/178/1/524/2069791 by guest on 12 March 2021

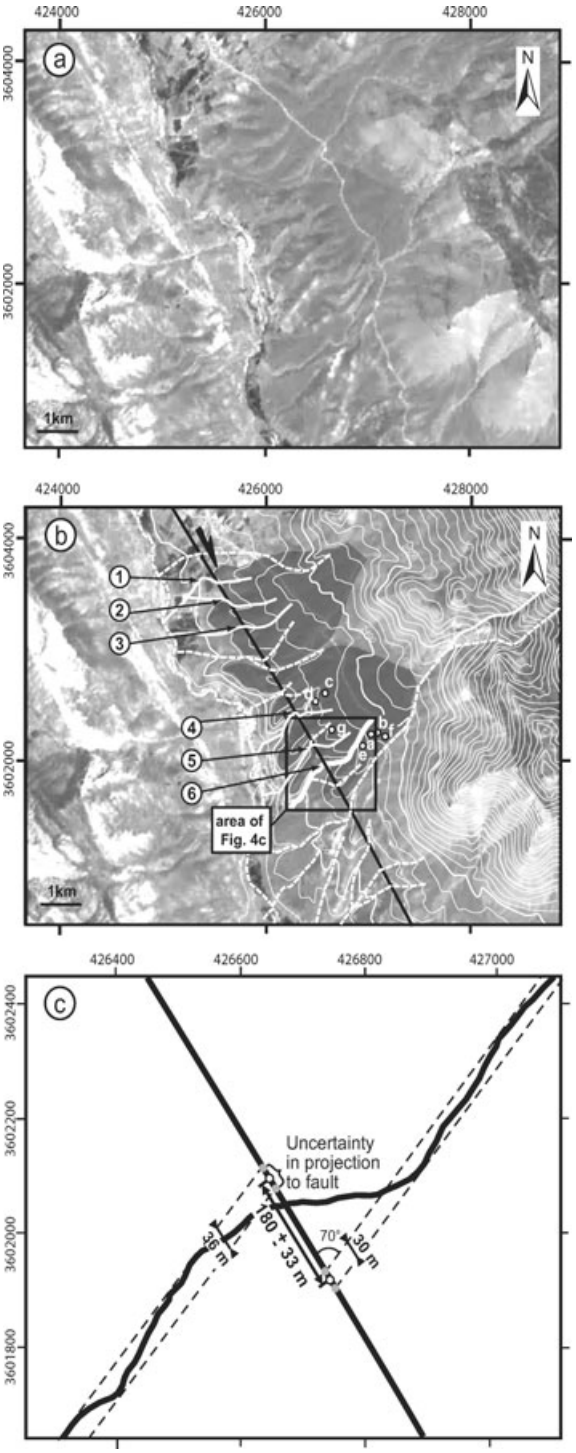


Figure 4. (a) 10-m resolution SPOT image of the Farsan segment of the Main Recent fault in the region of site 1 (coordinate system is in WGS 1984 UTM zone 39N). (b) Same image with superimposed 20 m contours (thin white lines) showing the two affected fans (grey surface) incised by deflected streams (white lines). Numbers indicate channel beds with comparable offsets (continuous white lines). Channels were extracted manually with an error of 10 m, reflecting the resolution of SPOT image. Bold white line is the differential GPS survey route of a selected stream. Dots and letters refer to the collected geochronological samples (Table 1). (c) Map view of the differential GPS survey along the selected stream and its lateral offset measurement.

two points on the fault. The southeasternmost point represents the point of the source stream the nearest to the fan apex. It is located in the clockwise bend of the stream against a shuttle ridge (Fig. 6b). The northwesternmost point is the intersection between the stream and the fault at the northwerternmost tip of the shuttle ridge (Fig. 6b). The uncertainty on the location of the two points accounts for the width of the stream (±5 m). Taking into account the uncertainty in the reconstruction of the fan's apex and the uncertainty given above, the measured tectonic lateral offset of the apex of the western fan ranges between 250 and 780 m (Fig. 6b).

4.2.2 Offset age and slip rates

We have sampled the eastern alluvial fan at site 2 for ^{36}Cl surface exposure dating (Figs 3b and 6a). Human induced reworking of the surface of the western fan prevented appropriate sampling. One distinguishes a group of four samples centred at ∼140 ka (Fig. 5a, Table 1). Three other samples lie well over this group with ages between 219 and 395 ka. A complementary depth profile was sampled on this fan from an excavation in order to estimate both the erosion rate and the exposure age of the alluvial surface through modelling of the *in situ* produced ^{36}Cl distribution with depth (Fig. 5b; Phillips *et al.* 2003; Siame *et al.* 2004). The modelled depth distribution was computed using all sources of production of chlorine 36 (Stone *et al.* 1998). Analysis of major elements and U and Th were done by ICP-OIS at CEREGE from an aliquot of the sample after crushing and sieving and were integrated in the model. Except for the sample taken at the surface, all points of the profile follow the theoretical exponential decrease. As the samples were collected in a pre-existing human made excavation, it is possible that the surface has been reworked in the first centimetres, which would explain the rather young age suggested by this surface sample. If we do not consider this sample in our modelling, the distribution is best explained by a surface exposure age between 150 and 250 ka and no erosion. The depth profile suggests exposure ages lying in between the two groups of ages deduced from the surface samples (Fig. 5). Moreover, both the depth profile samples and the three surface samples defining the oldest group have high natural chlorine concentrations (Table 1). It is therefore possible that those samples have undergone post-depositional thermal and epithermal neutron flux due to inhomogeneous snow cover, little cobble remobilization or burial (Bierman 1994; Liu *et al*. 1994). To summarize, the dating results from the surface samples and depth profile suggest that the surface of the fan remained nearly stable since its abandonment, which occurred between 121 and 169 ka ago.

The regional palaeoclimatic records and geomorphic observations compared with our dating can also provide further constrains on the abandonment age of the fan. Fan materials show gentle stratification without sedimentological sorting features of clasts and metric boulders in a sandy to silty matrix. These deposits can be viewed as debris-flow deposits that characterize fans in semi-arid environments (Nilsen 1982). The lack of moraine and glacial morphology of the valleys of the study area (Oberlander 1965) and the low fan surface slope gradient further suggest that the fans at site 2 are not humid-glacial fans (Ryder 1971). These fans compare to a primitive deposit of regional extent described in the southeasternmost Zagros fold-and-thrust belt. Geological, geomorphic and archeological data (Dufaure *et al.* 1977; Regard *et al.* 2005) indicate a Mid Pleistocene age for this deposit, during a humid period corresponding to the deglaciation between isotopic stages 6 and 5e, and before the onset of the last interglacial (∼125 ± 20 ka; Imbrie

Downloaded from https://academic.oup.com/gji/article/178/1/524/2069791 by guest on 12 March 2021

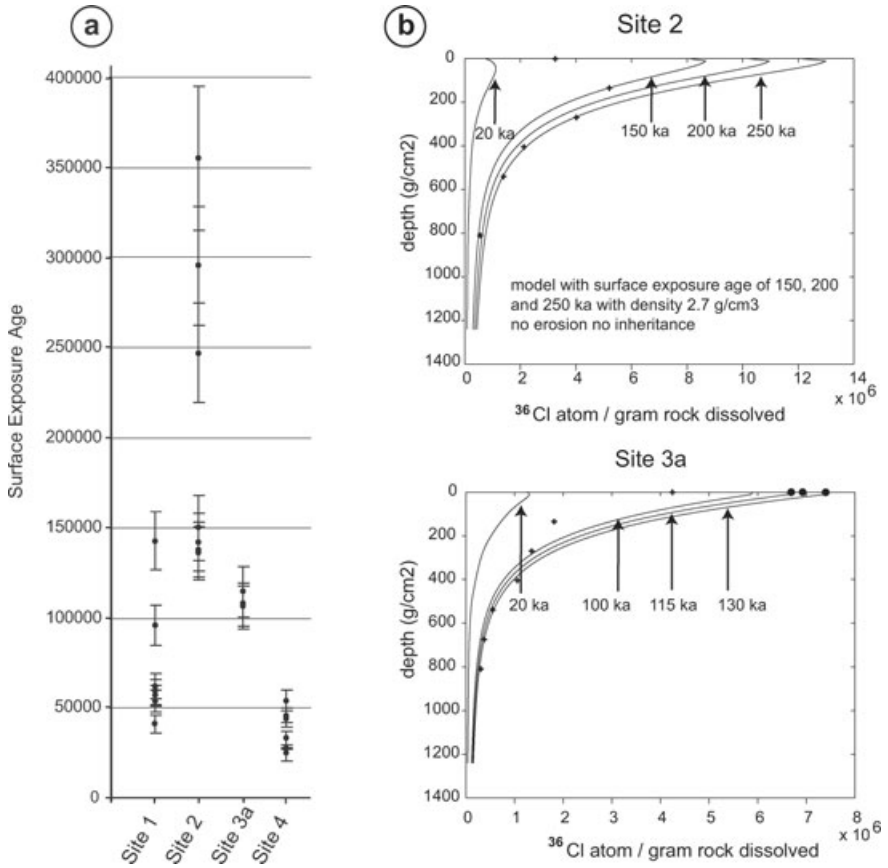


Figure 5. (a) Exposure ages of samples for each site, with corresponding error bars calculated assuming no erosion nor inheritance. (b) Depth profiles of ^{36}Cl concentration at site 2 and site 3a assuming a density of 2.7 g cm^{-3} for the model (samples have been collected every 50 cm). Crosses are ^{36}Cl concentrations versus depth, dots are surface exposure samples, lines are models with exposure ages of 20, 100, 115 and 130 ka, assuming no erosion and no inheritance.

et al. 1990). This humid period saw the expansion of forest trees in Northwestern Iran (Djamali *et al.* 2008) and led to the development of thick soils reflecting a pedogenic period during isotopic stage 5, as documented in the Persepolis basin, which lies 200 km from the study area (Kehl *et al.* 2005). This period between 105 and 145 ka is recorded, among others, by oxygen isotope record derived from speleothems at Pequiin and Soreq caves in Israel (Bar-Matthiews *et al*. 2003) and from speleothems at Hoti Cave in Northern Oman (Fleitmann *et al*. 2003). The first site was undergoing the influence of the Mediterranean climate at that time, whereas, contemporaneously, the second site saw the intertropical convergence zone moving north into the Arabian Peninsula at the time the Indian monsoon reached northern Oman (Burns *et al*. 2001). These considerations, together with the fact that ^{36}Cl surface exposure dating favours a fan exposure age between 121 ka and 169 ka, strengthen the assumption that fans of site 2 were emplaced during the warming event recognized around 105–145 ka (Imbrie *et al*. 1990) and more precisely around 125 ka in NW Iran (Djamali *et al.* 2008).

The cumulative right-lateral offset for the Ardal segment since the abandonment of the fans of site 2 ranges between 250 and 780 m. These values, combined with the fan abandonment age between 121 and 169 ka, leads to a slip rate of 1.5–6.5 mm yr^{-1} for the Ardal segment (Table 2).

4.3 Total slip rate on the main recent fault

As the Farsan and Ardal segments merge to the east and to the west, they must be linked at depth (Authemayou *et al.* 2006). Their respective slip rates must be added to obtain the total slip rate of the MRF. This yields a minimum right-lateral slip rate between 3.6 and 12.4 mm yr^{-1} on the MRF since the Late Pleistocene (Table 2).

5 SLIP RATES ON THE KAZERUN FAULT

5.1 Northern segment (site 3, 30°50′33 N, 51°28′05 E)

5.1.1 Offsets and age

The southern termination of the N-trending northern segment of the KF is bent towards the SE and splits into three faults (Figs 2 and 7a). In the vicinity of Sisarkht (site 3a), a large fan-terrace is affected by the two southernmost faults of this termination (Fig. 7a). The surface of the fan-terrace is capped by a calcrete that has preserved the fan from erosion. Field observations and differential GPS surveys with a decimetric resolution provide evidence for folding of the fan-terrace above the two faults (Figs 7b and c). The cumulated vertical offset of the fan surface by the two faults is 57 ± 1 m (Fig. 7c, Dv1 in Fig. 9). We did not detect any horizontal offset of, or within the fan-terrace at site 3a.

At site 3b, located 15 km to the NW of site 3a, the relict of a fan-terrace has the same position on the piedmont as that of the Sisarkht fan-terrace (site 3a). This geomorphic feature is offset by the main fault of the termination that could not be studied at site 3a (fault 2, Fig. 7a). The fan-terrace is both vertically and horizontally displaced by this fault (Fig. 8). Horizontal offset of 270–340 m

© 2009 The Authors, *GJI*, **178,** 524–540
Journal compilation © 2009 RAS

Downloaded from https://academic.oup.com/gji/article/178/1/524/2069791 by guest on 12 March 2021

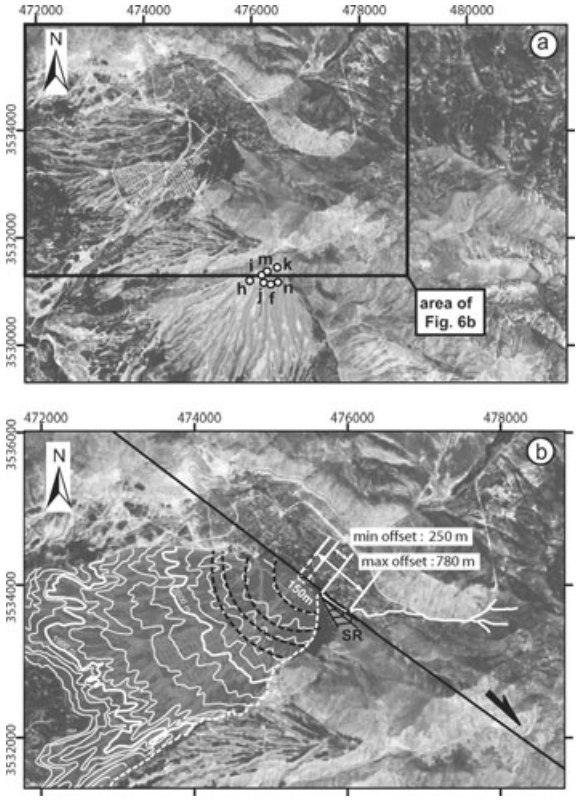


Figure 6. Morphotectonics of site 2 on the Ardal segment of the MRF. (a) 5-m resolution SPOT image showing the two studied alluvial fans (coordinate system is in WGS 1984 UTM zone 39N). Dots and letters refer to geochronological samples (Table 1). (b) 5-m resolution SPOT image focused on the western alluvial fan (grey surface). White line shows the source river valley of the alluvial fan. White dashed line shows today's downstream segment of the feeder valley. Concentric arcs fitting the fan's contours and their centres are represented by dotted black lines and white dots, respectively. SR, Shuttle ridge.

was measured using the displaced northwestern boundary of the fan-terrace and the deflection of a canyon incising the fan mapped on 15 m resolution ASTER images (Fig. 8b). The obtained value range corresponds to the maximum range of offsets of the two displaced markers by integrating the uncertainties associated with their extraction from the satellite image (Fig. 8b). The 40 ± 20 m vertical offset of the fan surface was obtained from the 20m-interval contours of the 1:50 000 topographic map (Fig. 8c).

The surface of the Sisarkht fan-terrace (site 3a) was sampled at three locations for ^{36}Cl exposure dating (Figs 7a and 3c). Assuming negligible erosion rates, the three samples give consistent exposure ages between 106 ± 12 and 115 ± 14 ka (Fig. 5, Table 1). We have also collected seven samples along a depth profile on the fan-terrace in a pre-existing excavation (Fig. 5b). The ^{36}Cl distribution is quasi-exponential, attesting to a homogeneous and single fan exposure history. Moreover, samples below 2 m depth have negligible ^{36}Cl concentrations suggesting the boulders forming this fan have very little inheritance. Except for the two samples near the surface, the best fit between the model and the data suggests an exposure age for the surface between 115 and 130 ka, in agreement with the surface exposure ages. As the depth profile samples were taken from a pre-existing excavation, it is possible that the surface has been reworked recently, which would explain why the two samples at the top of the profile did not fit the model. Although site 3b was not accessible for sampling, we assume that this fan-terrace was emplaced at the same time as that of site 3a, since those two fans have comparable geomorphic positions, incision pattern, surface appearance and roughness (Fig. 7a).

5.1.2 Slip rate

The horizontal displacement on the northern segment of the KF, which is a purely strike-slip fault (Authemayou *et al.* 2006), must equate the summation of the slip of the three strands studied at site 3 (Fig. 9). Therefore, the cumulated displacement along the faults of site 3a and 3b (Fig. 9) combined it with the fan-terrace exposure age provides an estimate of the slip rate on the northern segment of the KF. To calculate the cumulated displacement, we used the dip of the faults and the vertical and horizontal slip components of each faults obtained from the morphotectonic analysis (Fig. 9). The dip of the faults is derived from the balanced structural cross-section of Sherkati & Letouzey (2004) that crosses the studied area. On this section, the fault studied at site 3b is a basement fault that dips 70° to the north. The two fault strands studied at site 3a merge at depth to form a reverse fault dipping 40° to the north, which branches onto the basement fault. Based on these structural constraints, trigonometric calculation yields a cumulated displacement of 307–382 m along the northern segment of the KF since the abandonment of the fan-terraces (Fig. 9). Considering the

Table 2. Lateral tectonic offsets and corresponding slip rate estimates along the Main Recent Fault and the Kazerun Fault.

Fault	Site	Min lateral offset (m)	Max lateral offset (m)	Exposure age range Min age (yr)	Exposure age range Max age (yr)	Min slip rate (mm yr^{-1})	Max slip rate (mm yr^{-1})
MRF							
Farsan segment	1	147	213	36 000	69 000	2.1	5.9
Ardal segment	2	250	780	121 000	169 000	1.5	6.5
Farsan + Ardal segments						3.6	12.4
KF							
Northern segment	3a–3b	307	382	94 000	124 000	2,5	4,1
Central segment	5	65	85	22 000	60 000	1.1	3.9
	5	80	100			1.3	4.5
	5	70	90			1.2	4.1
	5	60	80			1.0	3.6
	5	90	110			1.5	5
Southern segment	12	0	0			0.0	0.0

Notes: The minimum and maximum horizontal offsets for each geomorphic marker take into account the errors inherent to the offset measurement and to the satellite images resolution. Minimum and maximum exposure ages at each site are determined from ^{36}Cl exposure ages distribution.

Downloaded from https://academic.oup.com/gji/article/178/1/524/2069791 by guest on 12 March 2021

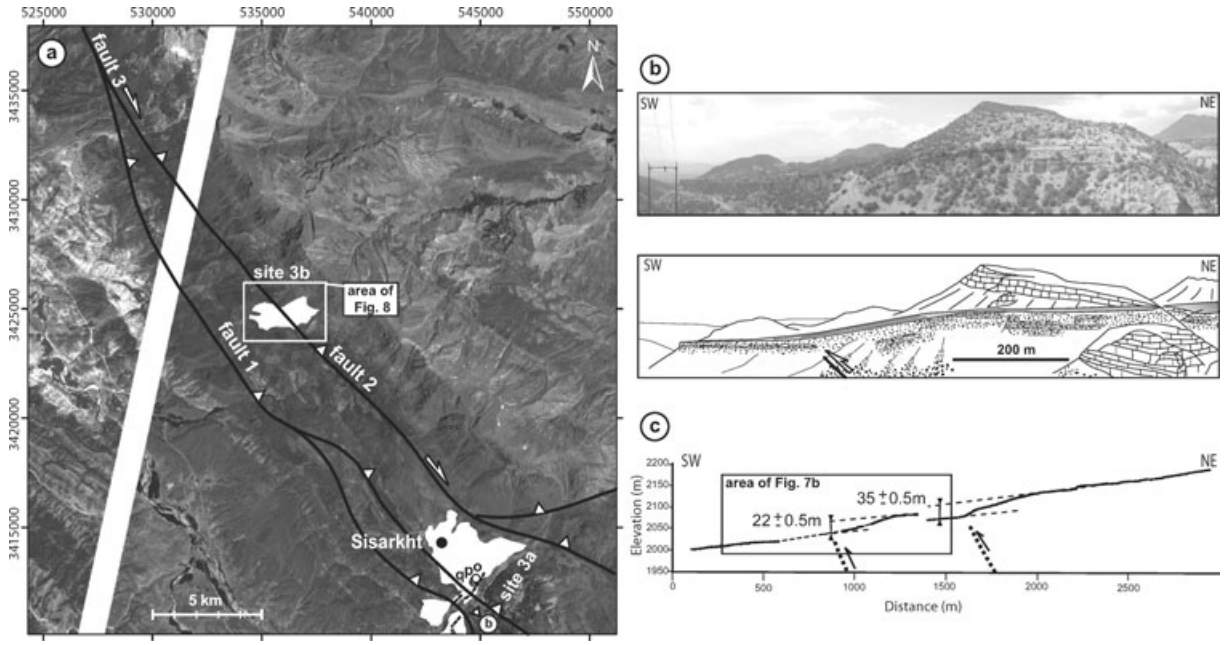


Figure 7. (a) Morphotectonics of sites 3a and 3b along the southern part of the northern segment of the Kazerun fault on a 15-m resolution ASTER image (See Fig. 2 for location) (coordinate system is in WGS 1984 UTM zone 39N). Fault traces are in black. The studied fan-terraces are in white. Differential GPS survey route is shown in black dotted line. Dots and letters refer to ^{36}Cl samples (Table 1). (b) West looking view of the anticline developed above the southern fault at site 3a. (c) Differential GPS topographic profile of the fan-terrace surface showing fault scarps at site 3a (located on Fig. 7a).

fan-terrace exposure age of 94–124 ka determined at site 3a, the minimum right-lateral slip rate for the Northern segment would be of 2.5–4.1 mm yr^{-1} (Table 2).

5.2 Central segment (sites 4, 29°52′61 N, 51°34′93 E and 5, 29°43′59 N, 51°30′68 E)

At site 5 (Fig. 2), two generations of Quaternary sedimentary deposits are crosscut by the fault (Fig. 10). An early pediment overlies the entire piedmont. It is made of poorly consolidated, reworked regolith rich in evaporitic concretions. Younger small alluvial fans were emplaced onto the surface of the pediment. These fans are made of dark silts that are intensively cultivated (Fig. 10). The southernmost fault trace is underlined by a 2 m-high scarp that affects the surface of the pediment just north of the Deylami village. The freshness of the scarp and a palaeoseismological trench in the close vicinity of the village (29° 45.952′N and 51° 31.541′E) provides evidence for at least two palaeoearthquakes during the Holocene (Bachmanov *et al*. 2004).

According to the GIS analysis of the SPOT image and the topographic map, three orders of magnitude of right-lateral geomorphic offsets may be recognized along the fault trace (Fig. 10b). The systematic asymmetry/dragging of the old drainage pattern entrenched in the pediment suggests offsets between 480 and 530 m. Along the two northern strands mapped on Fig. 10, apparent lateral offsets of large streams are of the order of 200–300 m. Smaller, systematic geomorphic offsets are recognized between the apexes of the dark, second-generation fans and their feeder source valleys or across the younger fans themselves. These offsets (including uncertainties) are comprised between *ca.* 60 and 110 m (Fig. 10, Table 2).

The absence of preserved pebbles at the surface of the old pediment and of the younger fans prevent ^{36}Cl surface exposure dating. However, the two fans emplaced on the same piedmont slope deposits 10 km further to the north (site 4; Fig. 2) may be seen as laterally equivalent to the younger fans from site 5 (Fig. 11). These fans are made of coarse-grained, highly heterogeneous debris-flow deposits, mainly made of limestone pebbles and boulders (Fig. 3d). The apexes of the fans lie against the single trace of the fault. Field observations of the fans'material and morphological relations, as well as the transverse topography of the deposits indicate that the two fans are contemporaneous and deposited above the abandonment surface of the old pediment (Fig. 11c). The two fans are covered by the same alluvial terrace as that of site 5. The geomorphic position of the younger fans at site 4 indicates that they are contemporaneous with the younger fans at site 5. The difference in the alluviums in the two contexts (silts in the South and cobbles in the North) is explained by the difference in the nature of the geological substrate of the two drainage basins that have fed the fans. Indeed, at site 5, bedrock is exclusively made of evaporites and marls whereas at site 4, bedrock is in part made of limestones (MacLeod & Majedi 1972). The surface exposure age of the fans at site 4 being the same as that of the fans at site 5, it can be used to compute a minimum slip rate on the fault measured at site 5.

The fan surface being unconsolidated, we have sampled large boulders ($\geq$1 m in diameter) that are not likely to have undergone postalluvial transport and that would reflect the surface abandonment age with negligible erosion since then (Figs 3d and 11a). Exposure ages of 7 samples range from 25 $\pm$ 3 ka to 53 $\pm$ 6 ka (Fig. 5, Table 1). The dispersion of the exposure ages could reflect successive emplacement episodes of distinct cobble populations. However, this age range overlaps that obtained at site 1 and may therefore be related to the same palaeoclimatic episode as that already reported in the southeasternmost Zagros by Regard *et al*. (2006). Combining minor fan offsets at site 5 (70–100 $\pm$ 10 m) with the full exposure age range obtained at site 5 yields lateral slip rates ranging between 1 and 5 mm yr^{-1} (Table 2). A common, realistic slip rate for the central segment of the KF is best described by a mean centred value of 1.5–3.6 mm yr^{-1} (Fig. 12).

Downloaded from https://academic.oup.com/gji/article/178/1/524/2069791 by guest on 12 March 2021

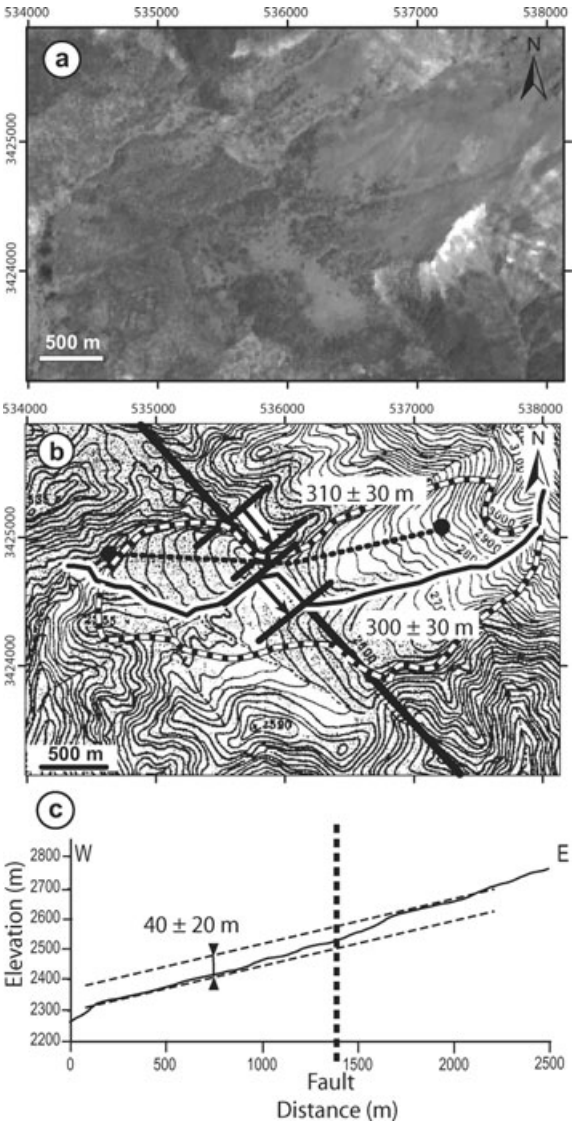


Figure 8. (a) 15 m resolution ASTER satellite image of site 3b (coordinate system is in WGS 1984 UTM zone 39N). (b) Geological interpretation and topography of (a) (20 m contours). Fan-terrace boundaries are shown by white dotted lines. The topographic profile of (c) is shown by a black dotted line, and the stream deflected by the fault is shown by a thick black and white line. Lateral offsets are shown by black arrows. The error in mapping the deflected stream and fan-terrace boundary is 15 m, accounting for the resolution of the ASTER image. The error in the offset measurement is 30 m. This distance is considered as the cumulative uncertainty on the locations of the two points used to measure the offset along the fault. (c) Topographic profile of the fan-terrace across the fault (located on b). The error in the vertical offset measurement depends on the contours of the topographic map (20 m).

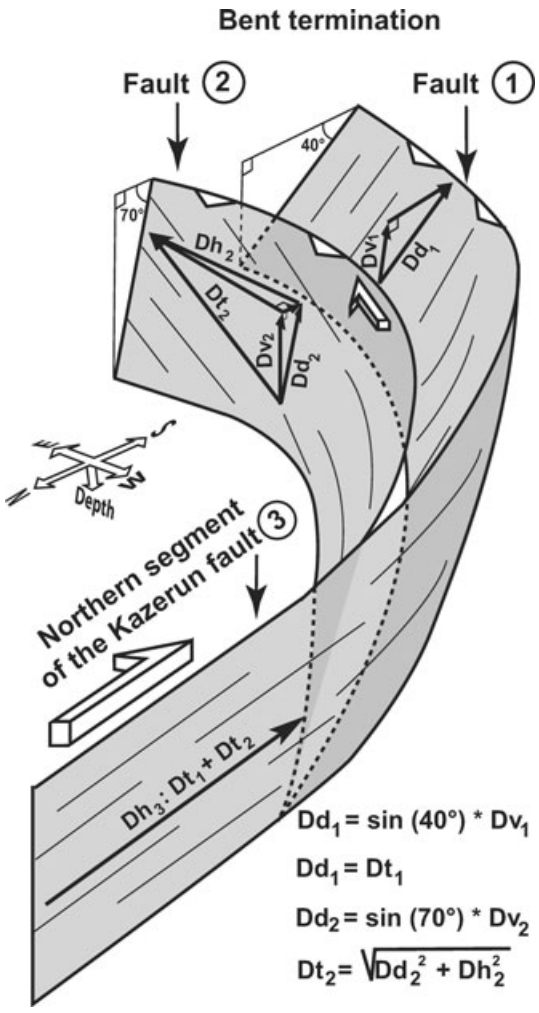


Figure 9. 3-D schematic representation of the northern segment of the Kazerun fault and its fault bent termination showing the distribution of the displacement on the various fault strands since fan-terrace abandonment at site 3 (Fig. 7). Fault 1 comprises the two strands studied at site 3a and fault 2 is the basement fault studied at site 3b (Figs. 7 and 8). Dh2 and Dh3 – horizontal component of slip along fault 2 and northern segment of the Kazerun fault (3), respectively; Dv1 and Dv2 – vertical component of slip along faults 1 and 2, respectively; Dd1 and Dd2 – downdip component of slip along faults 1 and 2, respectively; Dt1 and Dt2 – total slip along faults 1 and 2, respectively.

5.3 Southern segment

The southern segment consists in several faults making the western boundaries of anticlines arranged in an *en-échelon* pattern (Fig. 2). With the exception of a few pressure ridges, aerial photograph, topographic map, and SPOT satellite image analysis does not reveal apparent lateral distortion or offsets of geomorphic features along this segment. Evidence for present-day dominant dip-slip movements along the southern segment is attested by palaeoseismological data (Bachmanov *et al*. 2004) and by earthquake focal mechanisms (Talebian & Jackson 2004).

6 DISCUSSION

The present analysis indicates that the minimum late Quaternary slip rate on the MRF ranges from 3.5 to 12.5 mm yr^{-1}. The average value of this range is higher than that given by GPS measurements suggesting a right-lateral strike-slip rate across the whole central Zagros between 4 and 6 mm yr^{-1} (Fig. 13; Walpersdorf *et al*. 2006). Considering a N-trending instantaneous shortening rate of 7 ± 2 mm yr^{-1} in our study area and total partitioning of the convergence along the MRF, the maximum slip rate on the MRF should range between 3 and 7 mm yr^{-1} (Vernant *et al*. 2004a; Fig. 13a). Modelling of the GPS shortening rates by distributed transpression across the width of the fold-and-thrust belt would lead to a slip rate of

Downloaded from https://academic.oup.com/gji/article/178/1/524/2069791 by guest on 12 March 2021

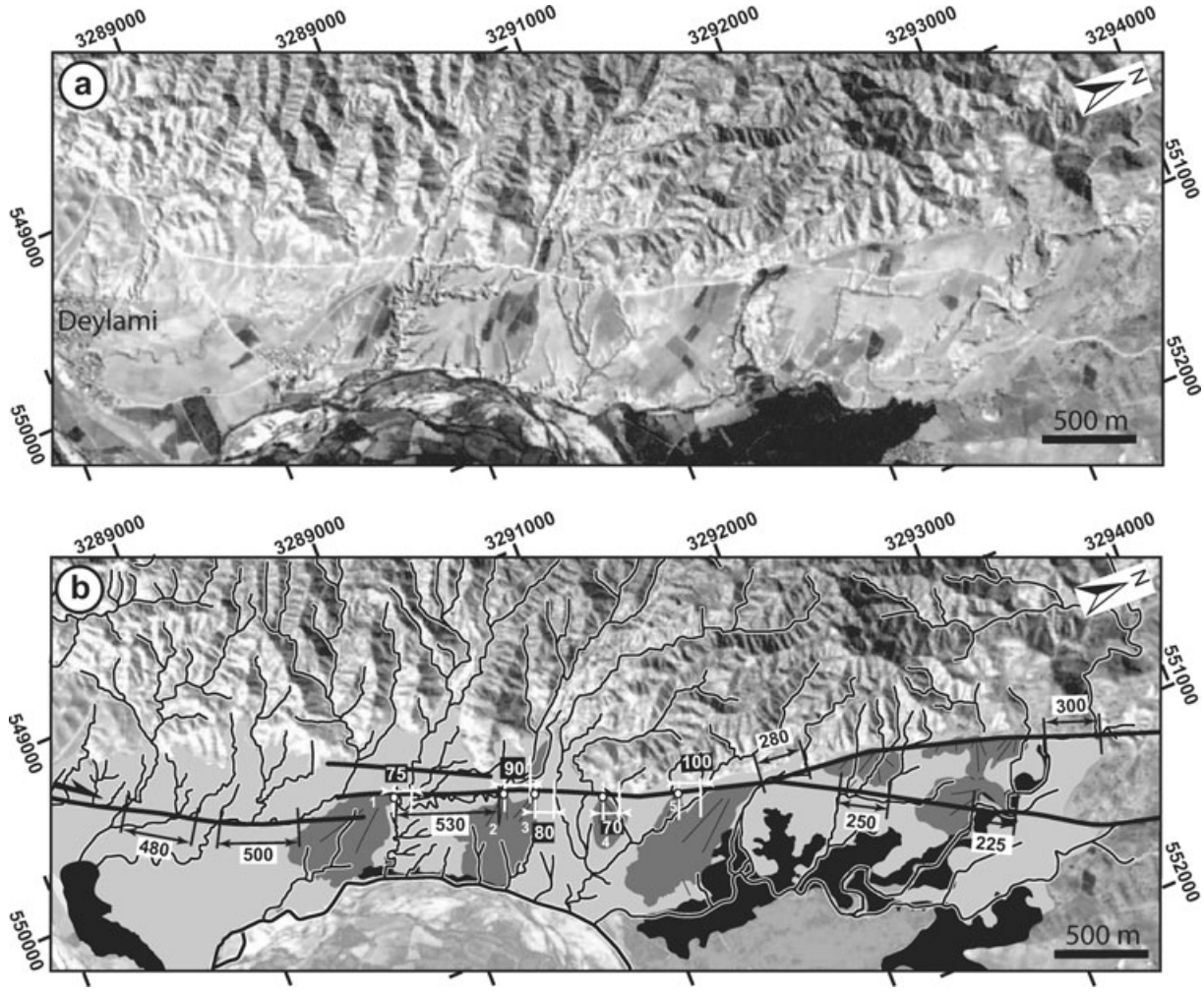


Figure 10. Morphotectonics of site 5 along the central segment of the Kazerun fault. (a) 5-m resolution SPOT satellite image (coordinate system is in WGS 1984 UTM zone 39N). (b) Quaternary geology and fault traces (black lines) of area mapped in (a). Early pediment deposits are shown in light grey and the younger alluvial fans in dark grey. White numbers refer to the offsets used to determine slip rates on Fig. 12. Younger alluvial terraces are in black. White dots and thin black lines indicate the apexes of the second-generation fans and their upstream valleys, respectively. These were extracted manually from the SPOT image and the topographic map with an error of 5 m, reflecting the resolution of SPOT image. The error in the offset measurement is 10 m. It is estimated as the cumulative uncertainty on the locations of the two points used to measure the offset along the fault. Measured geomorphic offsets are in metres.

1–2 mm yr^{-1} on the MRF (Vernant & Chéry 2006). Fault kinematics data complemented by morphotectonic study on the High Zagros fault indicate a transpressional regime (Malekzade *et al.* 2007). The lower bound of our slip rate estimate, together with the GPS data, suggest that the hypothesis of total partitioning along the MRF is valid. Clearly, our results, by providing the first direct constraint on the slip rate on the MRF over the Late Quaternary, imply significant partitioning along that fault.

The right-lateral slip rates obtained for the present work along the KF (2.5–4 mm yr^{-1} on the northern segment, 1.5–3.5 mm yr^{-1} on the central segment and negligible on the southern segment) is compatible with the slip rates determined by Tavakoli *et al*. (2008) from GPS survey (3.7 $\pm$ 0.8 mm yr^{-1} on the northern segment, 3.6 $\pm$ 0.6 mm yr^{-1} on the central segment and negligible on the southern segment). Given the geometrical and kinematic link between the MRF and the KF and the late Quaternary right-lateral slip rates reported here, up to 50 per cent of the slip on the MRF may be absorbed by the northernmost segment of the KF. The southward / longitudinal decrease in the right-lateral slip rate along the KF is interpreted to be due to the fact that part of that slip is progressively absorbed by the bent thrust termination of each segment of the KF. The dominant Late Quaternary reverse slip motion documented along the southern segment of the KF, which acts as the front of the southeastern Zagros, reflects a lateral fault ramp mechanism. The *en échelon* arrangement of the various strands of the southern segment further suggests southward propagation of the deformation front (e.g. Hessami *et al*. 2001; Sepehr & Cosgrove 2005). Prior to its present-day strike-slip regime, the KF was most likely already a lateral ramp. Considering a constant Quaternary slip rate, and combining the 1.5–3.5 mm yr^{-1} slip rate obtained here along the central segment of the KF with its finite lateral offset of 8 km determined by Authemayou *et al*. (2006) would yield to an age of 2–5 Ma for the onset of dominant strike-slip on the KF. This age is similar to that of the MRF (Talebian & Jackson 2002; Authemayou *et al.* 2006), supporting our interpretation that the KF was reactivated as a transcurrent fault as a consequence of the formation of the MRF (Authemayou *et al*. 2006).

West of the KF, the plate convergence rate of 7 $\pm$ 2 mm yr^{-1} (Vernant *et al.* 2004a) trending at 45° to the orogenic trend may be decomposed into an orogen-parallel component and an

© 2009 The Authors, *GJI*, **178,** 524–540
Journal compilation © 2009 RAS

Downloaded from https://academic.oup.com/gji/article/178/1/524/2069791 by guest on 12 March 2021

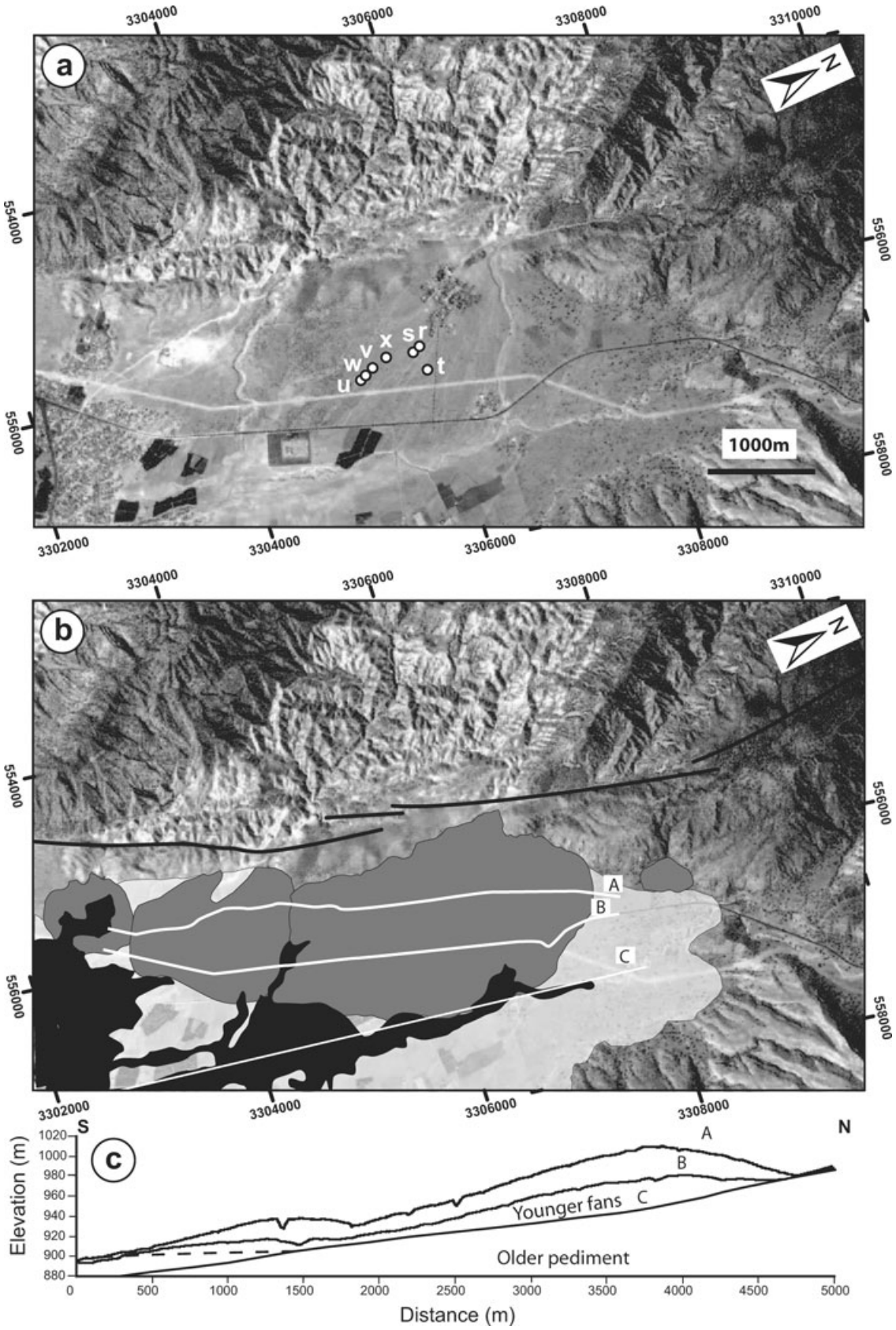


Figure 11. (a) SPOT satellite image of site 4 and its geological interpretation (b) on the central segment of the Kazerun fault (coordinate system is in WGS 1984 UTM zone 39N). Dots and letters refer to geochronological samples (Table 1). Fault traces are shown as black lines, the two younger fans are in dark grey. The old pediment underneath is shown in light grey. Black surface is the younger alluvial terrace. Differential GPS topographic profiles A, B and C are shown by white lines. (c) Differential GPS topographic profiles of the fans.

Downloaded from https://academic.oup.com/gji/article/178/1/524/2069791 by guest on 12 March 2021

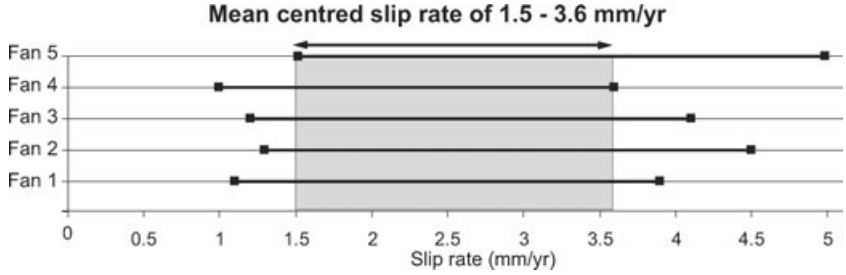


Figure 12. Minimum right-lateral slip rates of the central segment of the Kazerun fault. The graph shows individual slip rate ranges of the post-younger fans affected by the fault at site 5 that are distinguished by white numbers on Fig. 10 (Table 2). The width of each range reflects the errors on both the offset measurements on the satellite image and the abandonment age determinations from ^{36}Cl dating (Fig. 11, Table 1). As all these offsets are measured on the same fault strand and the fan abandonment surface has a single age, the fault must have a single slip rate since the onset of entrenchment of the drainage network. The representative horizontal slip rate (mean centred slip rate) is derived from the common value to each slip rate series (grey surface).

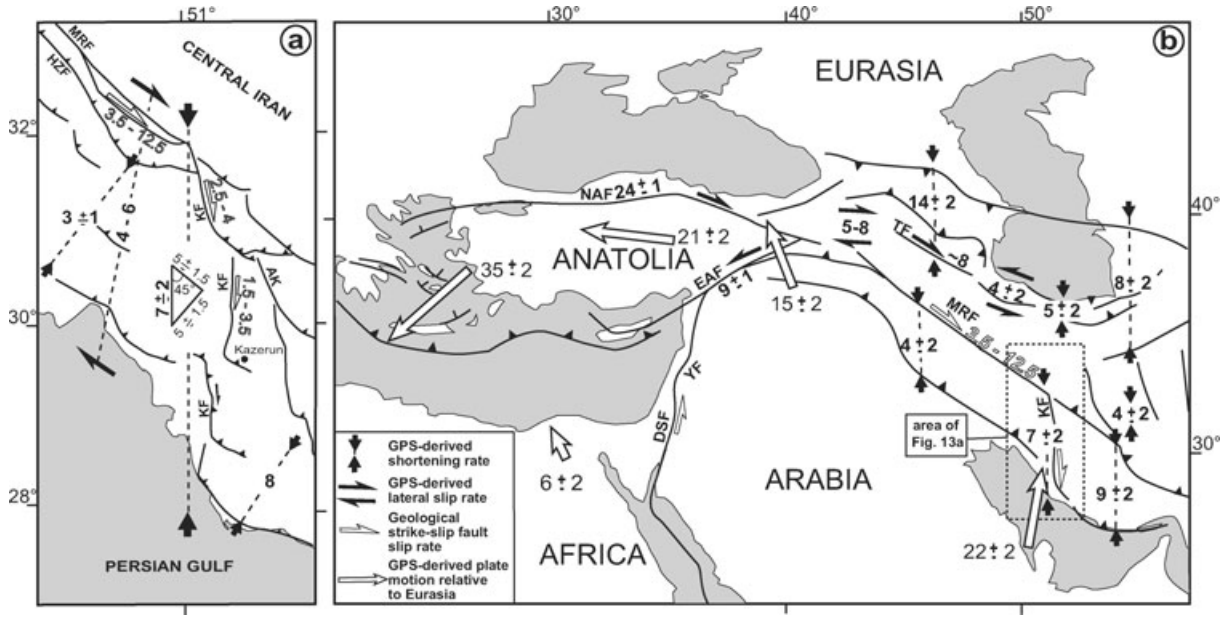


Figure 13. (a) Active deformation and slip rates (in mm yr^{-1}) in the Central part of the Zagros fold-and-thrust belt. Slip rates on the Main Recent Fault and Kazerun Fault are from the present study. (b) Active deformation and slip rates of the major faults of the Middle-East region. Lateral fault slip rates are either deduced from GPS data, late Quaternary dated offsets or long-term geological offsets (sources: Reilinger *et al.* 1997; McClusky *et al.* 2000; McClusky *et al.* 2003; Vernant *et al.* 2004a, b; Masson *et al.* 2006; Walpersdorf *et al*. 2006). Fault abbreviations: AK, Ardakan Fault; DSF, Dead Sea Fault; EAF, East Anatolian Fault; HZF, High Zagros Fault; KF, Kazerun Fault; MRF, Main Recent Fault; NAF, North Anatolian Fault; TF, Tabriz Fault; YF, Yammôuneh Fault.

orogen-normal component of 5 ± 1.5 mm yr^{-1} each (Fig. 13a). Southwest of the MRF, thrust faults have coseismic slip vectors striking normal to the structural trend of the belt (Talebian & Jackson 2004). Furthermore, the focal mechanisms along the MRF show pure strike-slip movements. This suggests that the orogen-parallel component of convergence is related to active strike-slip on the MRF and that the orogen-normal component of convergence is related to distribute dip-slip, orogen-normal thrusting in the fold-and-thrust belt. GPS data indicate that 3 ± 1 mm yr^{-1} of shortening are absorbed between the High Zagros Fault (HZF) and the coast (Walpersdorf *et al*. 2006), suggesting the remaining part of the 5 ± 1.5 mm yr^{-1} of shortening is absorbed between the MRF and the HZF.

East of the KF, most of the 8 mm yr^{-1} of instantaneous shortening is accommodated close to the Persian Gulf (Walpersdorf *et al*. 2006; Fig. 13a), indicating active shortening strain localization close to the front of the fold-and-thrust belt, as attested by the results of a recent morphotectonic study (Oveisi *et al.* 2009). This is also interpreted to reflect strain accumulation induced by the southern bent terminations of the fan-shaped strike-slip fault pattern that transfers slip from the MRF to the folds and thrusts of the belt, especially between the KF and the Ardakan Fault (Fig. 13a) and towards the front of the belt (Authemayou *et al.* 2006). To the southeast of the fan shaped fault pattern, in the absence of major strike-slip faults, the N–S overall shortening rate of 9 ± 2 mm yr^{-1} (Vernant *et al.* 2004a) is likely to be absorbed on the longitudinal thrusts and folds across the entire fold-and-thrust belt (Fig. 13b).

On a regional scale, the late Quaternary slip rate we have determined on the southeastern MRF is consistent with the overall right-lateral strike-slip rate of 5–8 mm yr^{-1} measured in Northwestern Iran from GPS data by Vernant *et al.* (2004a), and with the GPS-derived right-lateral slip rate on the Tabriz fault (∼8 mm yr^{-1}; Masson *et al.* 2006; Fig. 13b). The fact that the Tabriz fault and the dextral shear zone of Northwestern Iran achieve a significant amount of right-lateral strike-slip to the North and Northwest of the MRF (Fig. 13b) would be in agreement with the relatively small finite lateral offset of 10–15 km measured on that fault close to its northwestern termination by Copley & Jackson (2006).

© 2009 The Authors, *GJI*, **178,** 524–540
Journal compilation © 2009 RAS

Downloaded from https://academic.oup.com/gji/article/178/1/524/2069791 by guest on 12 March 2021

Even if the MRF may be seen as a southeastern extension of the North Anatolian Fault (NAF), the MRF slip rate is two to seven times smaller than that of the NAF (Bellier *et al*. 1997; Mc Clusky *et al.* 2000; Hubert-Ferrari *et al.* 2003; Fig. 13b). This is due to the westward tectonic escape of Anatolia enhanced by the slab retreat at the Hellenic subduction zone (Reilinger *et al*. 1997, Faccenna *et al.* 2006). Still, at the other end of the fault system, the fan shaped fault pattern making the termination of the MRF in southeastern Iran accommodates further propagation of the deformation front of the Zagros, which is enabled by the Cambrian salt detachment layer that underlies the sedimentary cover to the east of the KF. If the age of the MRF is Pliocene, the initiation of lateral slip on the NAF and MRF would be synchronous. Indeed, tectono-stratigraphic arguments and numerical modelling suggest that the NAF formed in the Middle or Late Miocene (Hubert-Ferrari *et al.* 2003, Sengör *et al*. 2005). Westward propagation of the NAF and formation of the current main strand of the East Anatolian Fault (EAF; Fig. 13) occurred in the Early Pliocene (∼5 Ma) and Late Early Pliocene (∼3 Ma), respectively (e.g. Sarağlu *et al.* 1992; Sengör *et al*. 2005). One may therefore tentatively relate the initiation of dominantly right-lateral slip on the KF at 2–5 Ma to the initiation of the NAF and EAF. The definitive acquisition of strike-slip partitioning in the Zagros fold-and-thrust belt by transfer of slip from the MRF to the KF must be seen as an effect of the regional reorganization of the Arabia-Eurasia collision that is inferred to have taken place at 5 ± 2 Ma by Allen *et al.* (2004). This regional reorganization may be associated with the break-off of the Arabian lithospheric slab (Molinaro *et al.* 2005; Authemayou 2006; Faccenna *et al.* 2006; Omrani *et al.* 2008).

7 CONCLUSION

The present study provides a Late Quaternary slip rate of 3.5–12.5 mm yr^{-1} on the Main Recent fault. Late Quaternary right-lateral slip rates along the Kazerun Fault are between 2.5 and 4 mm yr^{-1} for its northern segment, 1.5–3.5 mm yr^{-1} for the central segment and negligible for its southern segment. These results are consistent with southward distribution of the slip from along the Main Recent Fault to the longitudinal thrusts and folds of the fold-and-thrust belt through the Kazerun Fault and associated faults, with a decrease of slip from the southeastern tip of the Main Recent Fault towards the southeastern termination of the Kazerun Fault. Combined with GPS measurement results (Vernant *et al.* 2004a), our results suggest complete strike-slip partitioning of plate convergence in the Zagros on the Main Recent Fault. The Kazerun and associated faults form the horsetail termination of the MRF and may be seen as marking a propagating, southeasternmost front of the fault system that accommodates indentation of Eurasia by Arabia in the Caucasus.

ACKNOWLEDGMENTS

This work was supported by a cooperative research program between the CNRS (France) and the International Institute of Earthquake Engineering and Seismology (IIEES, Iran), supervised by D. Hatzfeld and M.G. Ashtyani. We thank the IIEES for fieldwork assistance and M. Mokhtari for support and administrative assistance. Funding was provided by the Intérieur de la Terre and Dyeti programs (INSU-CNRS), the IIEES and the CNRS via a sabbatical fellowship to D. Chardon. SPOT images were provided thanks to the ISIS program (©CNES 2000–2001-2002–2003, distribution SPOT images S.A.). We gratefully ackowledge R. Finkel at CAMS-LLNL who performed the ^{36}Cl measurements. We thank D. Bourlès, R. Braucher, J. Jackson, A. Walpersdorf, D. Hatzfeld, L. Palumbo and J. P. Ambrosi for fruitful discussions and help during the course of this work. The paper benefited from helpful reviews by R. Gloaguen, J. Jackson and O. Ritter.

REFERENCES

Allen, M.B., Jackson, J. & Walker, R., 2004. Late Cenozoic reorganization of the Arabia-Eurasia collision and the comparison of short-term and long-term deformation rates, *Tectonics,* **23,** TC2008, 1–16, doi:10.1029/2003TC001530.

Authemayou, C., 2006. Partitionnement de la convergence oblique en zone de collision: exemple de la chaîne du Zagros, *PhD thesis*. Univ. Paul Cézanne, Aix-Marseille, France, 334pp.

Authemayou, C., Bellier, O., Chardon, D., Malekzade, Z. & Abbassi, M., 2005. Role of Kazerun fault system in active deformation of the Zagros fold-and-thrust belt (Iran), *C.R. Géosci.,* **337**(5), 539–545.

Authemayou, C., Chardon, D., Bellier, O., Malekzade, Z., Shabanian, E. & Abbassi, M., 2006. Late Cenozoic partitioning of oblique plate convergence in the Zagros fold-and-thrust belt (Iran), *Tectonics,* **25,** TC3002, 1–21, doi:10.1029/2005TCOO1860.

Bachmanov, D.M., Trifonov, V.G., Hessami, Kh.T., Kozhurin, A.I., Ivanova, T.P., Rogozhin, E.A., Hademi, M.C. & Jamali, F.H., 2004. Active faults in the Zagros and Central Iran, *Tectonophysics,* **380,** 221–241.

Baker, C., Jackson, J. & Priestley, K., 1993. Earthquakes on the Kazerun line in the Zagros Mountains of Iran: strike-slip faulting within a fold-and-thrust belt, *Geophys. J. Int.,* **115,** 41–61.

Bar-Matthews, M., Ayalon, A., Gilmour, M., Matthews, A. & Hawkesworth, C.J., 2003. Sea–land oxygen isotopic relationships from planktonic foraminifera and speleothems in the Eastern Mediterranean region and their implication for paleorainfall during interglacial intervals, *Geochim. Cosmochim. Acta,* **67,** 3181–3199.

Bellier, O., Over, S., Poisson, A. & Andrieux, J., 1997. Recent temporal change in the stress and modern stress field along the North Anatolian Fault Zone, *Geophys. J. Int.,* **131,** 61–86.

Berberian, M., 1995. Master blind thrust faults hidden under the Zagros folds: active basement tectonics and surface morphotectonic, *Tectonophysics,* **241,** 193–224.

Berberian, M. & King, G.C.P., 1981. Towards a paleogeography and tectonic evolution of Iran, *Can. J. Earth Sci.,* **18,** 210–285.

Berberian, M. & Tchalenko, J., 1976. Earthquakes of the southern Zagros (Iran): Bushehr region, *Geol. Surv. Iran Mem.,* **39,** 343–370.

Berberian, M. & Yeats, R.S., 2001. Contribution of archaeological data to studies of earthquake history in the Iranian Plateau, *J. Struct. Geol.,* **23,** 563–584.

Bierman, P.R., 1994. Using *in situ* produced cosmogenic isotopes to estimate rates of landscape evolution: a review from the geomorphic perspective, *J. geophys. Res.,* **99**(B7), 13 885–13 896.

Burns, S.J., Fleitmann, D., Matter, A., Neff, U. & Augusto, M., 2001. Speleothem evidence from Oman for continental pluvial events during interglacial periods, *Geology,* **29,** 623–626.

Cerling, T.E. & Craig, H., 1994. Geomorphology and in-situ cosmogenic isotopes, *Ann. Rev. Earth planet. Sci.,* **22,** 273–317.

Copley, A. & Jackson, J., 2006. Active Tectonics of the Turkish-Iranian Plateau, *Tectonics,* **2,** TC6006, 1–19, doi:10.1029/2005TC001906.

Daeron, M., Benedetti, L., Tapponnier, P., Sursock, A. & Finkel, R.C., 2004. Constraints on the post 25-ka slip rate of the Yammoûneh fault (Lebanon) using *in situ* cosmogenic ^{36}Cl dating of offset limestone-clast fans, *Earth planet. Sci. Lett.,* **227**(1–2), 105–119.

Djamali, M. *et al*., 2008. A late Pleistocene long pollen record from Lake Urmia, NW Iran, *Quater. Res.,* **69,** 413–420.

Dufaure, J.J., Thibault, C., Kadjar, M.H. & Mercier, J.L., 1977. La zone de faille de Zendan (Iran du Sud-Est): I – Géomorphologie et stratigraphie du Quaternaire, *Paper presented at Réunion Annuelle des Sciences de la Terre (6th RAST)*, Soc. Géol. de Fr., Orsay, France.

Downloaded from https://academic.oup.com/gji/article/178/1/524/2069791 by guest on 12 March 2021

Faccenna, C., Bellier, O., Martinod, J., Piromallo, C. & Regard, V., 2006. Slab detachment beneath eastern Anatolia: a possible cause for the formation of the North Anatolian fault, *Earth planet. Sci. Lett.,* **242,** 85–97.

Falcon, N.L., 1969. Problem of the relationship between surface structures and deep displacement illustrated by the Zagros range, in *Time and Place in Orogeny,*Vol. 3, pp. 9–22, eds Kent, P.E., Satterwaite, G.E. & Spencer, A.M., *Geol. Soc. Spec. Publ.*

Falcon, N.L., 1974. Southern Iran: Zagros mountains, in *Mesozoic-Cenozoic Orogenic Belts, Data for Orogenic Studies,*Vol. 4, pp. 199–211, ed. Spencer, A.M., *Geol. Soc. Spec. Publ.*

Fleitmann, D., Burns, S.J., Neff, U., Mangini, A. & Matter, A., 2003. Changing moisture sources over the last 330000 years in Northern Oman from fluid-inclusion evidence in speleothems, *Quater. Res.,* **60,** 223–232.

Gosse, J.C. & Phillips, F.M., 2001. Terrestrial *in situ* cosmogenic nuclides: theory and application, *Quater. Sci. Rev.,* **20,** 1475–1560.

Haynes, S.J. & McQuillan, H., 1974. Evolution of the Zagros Suture Zone, Southern Iran, *Geol. Soc. Am. Bull.,* **85,** 739–744.

Hessami, K., Koyi, H.A., Talbot, C.J., Tabasi, H. & Shabanian, E., 2001. Progressive unconformities within an evolving foreland fold-thrust belt, Zagros mountains, *J. Geol. Soc. Lond.,* **158,** 969–981.

Hessami, K., Nilforoushan, F. & Talbot, C., 2006. Active deformation within the Zagros Mountains deduced from GPS measurements, *J. Geol. Soc. Lond.,* **163,** 143–148.

Hubert-Ferrari, A., King, G., Manighetti, I., Armijo, R., Meyer, B. & Tapponnier, P., 2003. Long-term elasticity in the continental lithosphere; modelling the Aden Ridge propagation and the Anatolian extrusion process, *Geophys. J. Int.,* **153,** 111–132.

Imbrie, J., McIntyre, A. & Mix, A.C., 1990. Oceanic response to orbital forcing in the Late Quaternary: observational and experimental strategies, in *Climate and Geosciences, A Challenge for Science and Society in the 21st Century,* eds Berger, A., Schneider, S.H. & Duplessy, J.-C.D., Reidel Publishing Company, Boulder, CO, USA.

Jackson, J. & McKenzie, D.P., 1984. Active tectonics of the Alpine-Himalayan belt between western Turkey and Pakistan, *Geophys. J. R. astr. Soc.,* **77,** 185–264.

Jackson, J.A. & McKenzie, D.P., 1988. The relationship between plate motion and seismic moment tensors, and the rates of active deformation in the Mediterranean and Middle East, *Geophys. J. R. astr. Soc.,* **93,** 45–73.

James, G.A. & Wynd, J.G., 1965. Stratigraphic nomenclature of Iranian oil consortium agreement area, *AAPG Bull.,* **49,** 2162–2245.

Kehl, M., Frechen, M. & Skowronek, A., 2005. Paleosols derived from loess and loess-like sediments in the Basin of Persepolis, *Southern Iran, Quater. Int.,* **140–141,** 135–149.

Keller, E.A., Seaver, D.B., Laduzinsky, D.L., Johnson, D.L. & Ku, T.L., 2000. Tectonic geomorphology of active folding over buried reverse faults: San Emigdio Mountain front, southern San Joaquin Valley, California, *Geol. Soc. Am. Bull.,* **112**(1), 86–97.

Liu, B., Phillips, F.M., Fabryka-Martin, J.T., Fowler, M.M. & Stone, W.D., 1994. Cosmogenic ^{36}Cl accumulation in unstable landforms, 1. Effects of the thermal neutron distribution, *Water Resour. Res.,* **30,** 3115–3125.

MacLeod, J.H. & Majedi, M., 1972. *Geological Map of Iran,* Kazerun sheet (NO.20846), scale 1:100,000, Natl. Iran. Oil Co., Tehran.

Malekzade, Z., Abbassi, M.R., Bellier, O. & Authemayou, C., 2007. Strain Partitioning in West-Central Zagros Fold and Thrust Belt: implication for Seismic Hazard Analysis, *JSEE,* **9,** 85–98.

Masson, F., Van Gorp, S., Chéry, J., Djamour, Y., Tatar, M., Tavakoli, F., Nankali, H. & Vernant, P., 2006. Extension in NW Iran driven by the motion of the south Caspian basin, *Earth planet. Sci. Lett.,* **252,** 180–188.

McClusky, S.M. *et al*., 2000. Global Positioning System constrains on plate kinematics and dynamics in the eastern Mediterranean and Caucasus, *J. geophys. Res.,* **105**(B3), 5695–5719.

McClusky, S.M., Reilinger, R., Mahmoud, S., Ben Sari, D. & Tealeb, A., 2003. GPS constraints on Africa (Nubia) and Arabia plate motions, *Geophys. J. Int.,* **155,** 126–138.

Molinaro, M., Zeyen, H. & Laurencin, X., 2005. Lithospheric structure underneath the south-eastern Zagros mountains, Iran: recent slab break-off? *Terra Nova,* **17,** 1–6.

Nilsen, T.H., 1982. Alluvial fan deposits, in *Sandstone Depositional Environments,*Vol. 31, pp. 49–86, eds Scholle, P.A. & Spearing, D. *AAPG Mem*.

Oberlander, T., 1965. The Zagros stream: a new interpretation of Transverse Drainage in an Orogenic Zone, *Syracuse Geogr. Ser.,* **1,** 1–168.

Omrani, J., Agard, P., Whitechurch, H., Benoit, M., Prouteau, G. & Jolivet, J., 2008. Arc-magmatism and subduction history beneath the Zagros Mountains, Iran: a new report of adakites and geodynamic consequences, *Lithos,* **106,** 380–398.

Oveisi, B., Lavé, J., Van Der Beek, P., Carcaillet, J., Benedetti, L. & Aubourg, C., 2009. Thick- and thin-skinned deformation rates in the central Zagros simple folded zone (Iran) indicated by displacement of geomorphic surfaces, *Geophys. J. Int.,* **176,** 627–654.

Peyret, M., Rolandone, F., Dominguez, S., Djamour, Y. & Meyer, B., 2008. Source model for the Mw 6.1, 31 March 2006, Chalan-Chulan Earthquake (Iran) from InSAR, *Terra Nova,* **20,** 126–133.

Phillips, F.M., Ayarbe, J.P., Bruce, J., Harrison, J. & Elmore, D., 2003. Dating rupture using cosmogenic nuclides and scarp morphology, *Earth planet. Sci. Lett.,* **215,** 203–218.

Regard, V. *et al*., 2005. Cumulative right-lateral fault slip rate across the Zagros–Makran transfer zone and role of the Minab-Zendan fault system within the convergence accommodation between Arabia and Eurasia (SE Iran), *Geophys. J. Int.,* **160,** 1–25.

Regard, V. *et al*., 2006. ^{10}Be dating of alluvial deposits from Southeastern Iran (the Hormoz Strait area), *Paleogeogr. Palaeoclim. Palaeoecol.,* **242,** 36–53.

Reilinger, R.E. *et al*., 1997. Global positioning System measurements of present-day crustal movements in the Arabia-Africa-Eurasia plate collision zone, *J. geophys. Res.,* **102**(B5), 9983–9999.

Ricou, L.E., Braud, J. & Bruhnn, J.H., 1977. Le Zagros, *Mem. H. Sér. Soc. Géol. Fr.,* **8,** 33–52.

Ryder, J.M., 1971. The stratigraphy and morphology of paraglacial alluvials fans in south-central British Columbia, *Can. J. Earth Sci.,* **8,** 279–298.

Saraǧlü, F., Emre, Ö. & Kuşçu, I., 1992. The East Anatolian Fault of Turkey, *Ann. Tectonicae,* **6,** 125–199.

Schwartz, D.P. & Sibson, R.H., 1989. Fault segmentation and controls of rupture initiation and termination, in *USGS Open-File Report 89315,* 445 pp., eds Schwartz, D.P. & Sibson, R.H., USGS.

Şengör, A.M.C., Tüysüz, O., İmren, C., Sakinç, M., Eyidoğan, H., Görür, N., Le Pichon, X. & Rangin, C., 2005. The North Anatolian Fault: a new Look, *Ann. Rev. Earth planet. Sci.,* **33,** 37–112.

Sepehr, M. & Cosgrove, J.W., 2005. Role of the Kazerun Fault zone in the formation and deformation of the Zagros Fold-Thrust Belt, *Iran, Tectonics,* **24,** TC5005, 1–13, doi:10.29/2004TC001725.

Sherkati, S. & Letouzey, J., 2004. Variation of structural style and basin evolution in the central Zagros (Izeh zone and Dezful Embayment), *Iran, Mar. Petrol. Geol.,* **21,** 535–554.

Siame, L. *et al*., 2004. Local erosion rates versus active tectonics: cosmic ray exposure modelling in Provence (south-east France), *Earth planet. Sci. Lett.,* **7010,** 1–20.

Stöcklin, J., 1968. Structural history and tectonics of Iran. A review, *AAPG Bull.,* **52,** 1229–1258.

Stöcklin, J., 1974. Possible ancient continental margins in Iran, in *The Geology of Continental Margins,* pp. 873–877, eds Burke, C.A. & Drake, C.L., Springer-Verlag, New York.

Stone, J.O., Evans, J.M., Fifield, L.K., Allan, G.L. & Cresswell, R.G., 1998. Cosmogenic chlorine-36 production in calcite by muons, *Geochim. Cosmochim. Acta,* **62,** 433–454.

Stone, J.O., 2000. Air pressure and cosmogenic isotope production, *J. geophys. Res.,* **105**(B10), 23 753–23 759, doi:10.1029/2000JB900181.

Stoneley, R., 1981. The geology of the Kuh-e Dalneshin area of southern Iran, and its bearing on the evolution southern Tethys, *J. Roy. Soc. Lond.,* **138,** 509–526.

Swanson, T.W. & Caffee, M.L., 2001. Determination of ^{36}Cl production rates derived from the well-dated deglaciation surfaces of Whidbey and Fidalgo Islands, *Washington, Quater. Res.,* **56,** 366–382.

Talebian, M. & Jackson, J., 2002. Offset on the Main Recent Fault of the NW Iran and implications for the late Cenozoic tectonics of the Arabia-Eurasia collision zone, *Geophys. J. Int.,* **150,** 422–439.

Downloaded from https://academic.oup.com/gji/article/178/1/524/2069791 by guest on 12 March 2021

Talebian, M. & Jackson, J., 2004. A reappraisal of earthquake focal mechanisms and active shortening in the Zagros mountains of Iran, *Geophys. J. Int.,* **156,** 506–526.

Tatar, M., Haztfeld, D., Martinod, J., Walpersdorf, A., Ghafori-Ashtiany, M. & Chéry, J., 2002. The present-day deformation of the central Zagros from GPS measurements, *Geophys. Res. Lett.,* **29**(19), 1927, 33.1–33.4, doi:10.1029/2002GL015427.

Tavakoli, F. *et al*., 2008. Distribution of the right-lateral strike–slip motion from the Main Recent Fault to the Kazerun Fault System (Zagros, Iran): evidence from present-day GPS velocities, *Earth planet. Sci. Lett.,* **275,** 342–347.

Tchalenko, J.S. & Braud, J., 1974. Seismicity and structure of Zagros (Iran): the Main Recent Fault between 33° and 35°N, *Philos. Trans. R. Soc. Lond.,* **277,** 1–25.

Tibaldi, A. & Leon, J.R., 2000. Morphometry of late Pleitocene-Holocene faulting and volcanotectonic relationship in the southern Andes of Colombia, *Tectonics,* **19,** 358–377.

Vernant, P. *et al*., 2004a. Contemporary crustal deformation and plate kinematics in Middle East constrained by GPS measurements in Iran and northern Oman, *Geophys. J. Int.,* **157,** 381–398.

Vernant, P. *et al*., 2004b. Deciphering oblique shortening of central Alborz in Iran using geodetic data, *Earth planet. Sci. Lett.,* **223,** 117–185.

Vernant, P. & Chéry, J., 2006. Mechanical modelling of oblique convergence in the Zagros, Iran, *Geophys. J. Int.,* **165,** 991–1002.

Walpersdorf, A. *et al*., 2006. Comparison of the North and Central Zagros present day formation observed by GPS, *Geophys. J. Int.,* **167,** 1077–1088.

Yamini-Fard, F., Hatzfeld, D., Tatar, M. & Mokhtari, M., 2006. Microearthquake seismicity at the intersection between the Kazerun fault and the Main Recent Fault (Zagros, Iran), *Geophys. J. Int.,* **166,** 186–196.

Downloaded from https://academic.oup.com/gji/article/178/1/524/2069791 by guest on 12 March 2021